iScience

Article

Unraveling the aging-reversal potency of stem cell-derived extracellular vesicles in a rat model of premature cardiac senescence

Graphical abstract

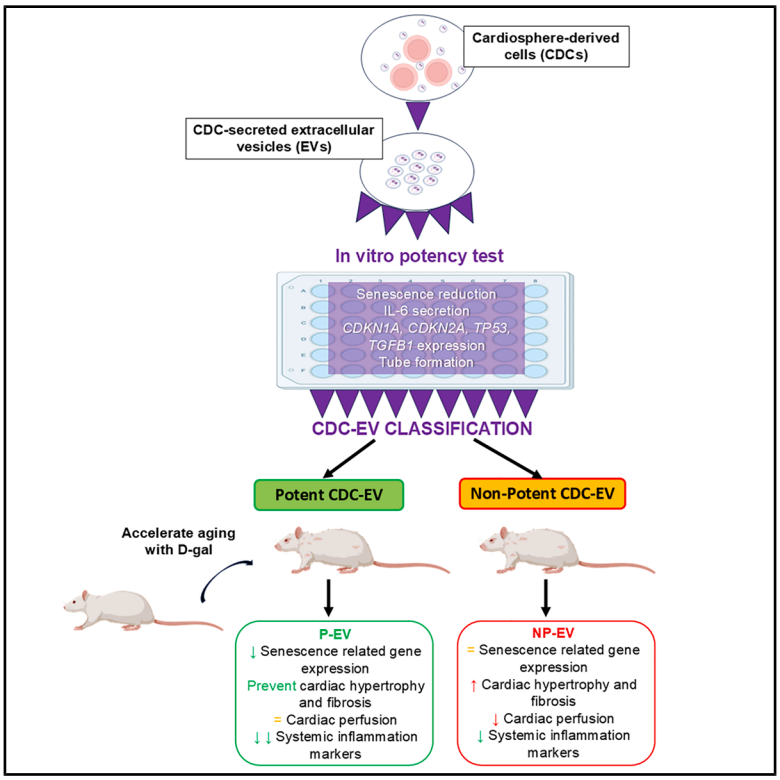

Highlights

- Phenotypically similar EVs show different *in vitro* and *in vivo* bioactivity
- Donor's age does not determine CDC-EVs' anti-aging potency
- *In vitro* bioactivity in our potency assay can predict *in vivo* effects of EVs
- Potent CDC-EVs in the assay show more rejuvenating potential in cardiac aging

Authors

Lidia Gómez-Cid,
Alexia Campo-Fonseca,
Mar Cervera-Negueruela, ...,
Susana Suárez-Sancho,
Francisco Fernández-Avilés,
Lilian Grigorian-Shamagian

Correspondence

grigorianl@yahoo.es

In brief

Biological sciences; Cell biology; Biological sciences research methodologies

Gómez-Cid et al., 2025, iScience *28*, 112910
July 18, 2025
https://doi.org/10.1016/j.isci.2025.112910

CellPress

iScience

CellPress
OPEN ACCESS

Article

Unraveling the aging-reversal potency of stem cell-derived extracellular vesicles in a rat model of premature cardiac senescence

Lidia Gómez-Cid,[1] Alexia Campo-Fonseca,[1] Mar Cervera-Negueruela,[1] Alejandra Ocampo,[2] Ángel Pinto,[3] Juan Miguel Gil-Jaurena,[3] Susana Suárez-Sancho,[2] Francisco Fernández-Avilés,[4,5] and Lilian Grigorian-Shamagian[5,6,*]

[1]Departamento de Bioingeniería, IiSGM, Universidad Carlos III de Madrid, 28911 Leganés, Spain
[2]Unidad de Producción Celular, Hospital General Universitario Gregorio Marañón, 28009 Madrid, Spain
[3]Hospital General Universitario Gregorio Marañón, 28009 Madrid, Spain
[4]Faculty of Medicine, Universidad Complutense de Madrid, 28040 Madrid, Spain
[5]Cardiology Department, San Rafael University Hospital, Universidad Francisco de Vitoria, Madrid, Spain
[6]Lead contact
*Correspondence: grigorianl@yahoo.es
https://doi.org/10.1016/j.isci.2025.112910

SUMMARY

Cardiosphere-derived cells (CDCs) and their extracellular vesicles (CDC-EVs) can rejuvenate and improve cardiac function, but their efficacy varies among donors. This study aimed to identify predictors of CDC-EV potency. CDCs from human donors were analyzed for phenotypical and biological properties. The anti-aging activity of CDC-EVs was tested using an *in vitro* matrix assay. Results showed that donor age did not determine potency, but CDC senescence correlated with most bioactive properties. However, senescence alone was insufficient to predict CDC-EV potency. CDC-EVs were classified as more potent (P-EVs) or less potent (NP-EVs) based on assay performance. In a rat model of premature cardiac aging, P-EVs reduced senescence-associated *GLB1* gene expression and protected against hypertrophy and fibrosis, while NP-EVs had negative effects. The study concludes that CDC-EV anti-aging potency cannot be predicted by donor age or CDC senescence, proposing an *in vitro* potency assay for evaluating CDC-EVs before clinical use.

INTRODUCTION

Cellular, structural, and functional changes associated to aging are largely responsible for heart diseases such as heart failure with preserved ejection fraction (HFpEF).[1] HFpEF remains an unmet medical need because of its increasing prevalence, high mortality and morbidity rates, and limited therapeutic strategies available.[2,3] Cardiac aging is associated with increased cell senescence,[4–6] compromised myocardial perfusion,[7] and increased fibrosis and hypertrophy[8] among others. Cardiosphere-derived cells (CDCs) and the extracellular vesicles they release (CDC-EVs) present promising characteristics for reverting some of these aging-associated pathological features[9] as demonstrated in preclinical studies,[10,11] such as increasing microvessel formation,[12] attenuating cardiomyocyte apoptosis and hypertrophy, reducing regional fibrosis,[13,14] and acting as immunomodulators.[13,15] Cardiospheres are self-organized three-dimensional (3D) structures obtained after established 3D culturing system from cardiac explant-derived cells (EDCs).[16] Cardiospheres are a complex, niche-like environment that favors proliferation and stemness of cardiac progenitor cells. CDCs, obtained after further culture of cardiospheres, are multipotent and clonogenic.[17] They express CD105 and are negative for the expression of hematopoietic markers (CD45).[16] Inside the CDC population, there are a variable proportion of cells expressing other surface markers: CD117 (c-kit), CD90 (Thy-1), and CD31.[16] Therefore, they include different subpopulations such as c-kit+ cells, endothelial cells, and mesenchymal stem cells. In clinical trials, the use of CDCs has been proven to be safe and to have some beneficial effects.[18–20]

However, when moving stem cells or extracellular vesicles as products from the preclinical to the clinical scenario, the results are less satisfactory than expected.[21] Hasty translation led to underestimation of how the heterogeneity and complexity of these products could impact their potency,[22] one of the factors that could influence the disappointing results of previous clinical trials.[23] Although most clinical trials in the field used confirmation of cell identity as the single requirement before product administration,[24] the gold standard for cell potency assessment in cardiac applications is structural and functional recovery in a rodent model of myocardial infarction.[25,26] However, this model is costly, time-consuming, and of doubtful translation, hindering its use for routine testing.[27] *In vitro* functional assays do not reflect the complexity of living organisms, but they require less time and economic resources and can be representative of the potential mechanism of action (MoA) of the tested product if

properly validated. Finding economic, feasible, and efficient potency assays based on evidence of MoA for therapeutic cells and cell-derived EVs in the cardiovascular field still remains a challenge[24,28,29] and crucial for successful translation.

Considering relevant characteristics and the potential MoA by which CDC-EVs may exert their beneficial effects in the treatment of cardiac aging, we here explore if the donors' chronological age, senescence of the CDCs, and/or CDC-EV rejuvenating potency *in vitro* can be used to predict CDC-EV efficacy *in vivo*.

RESULTS

The senescence status more than the chronological age of cell donors determines the cardiosphere-derived cells bioactivity

CDC senescence seemed more determinant of CDCs' proliferative and migrative properties in culture than cardiac tissue donors' chronological age. An example of CDCs' properties from a chronologically aged donor (70-years old) but with "low" senescence rate in culture (9.1%) vs. a chronologically young donor (7-months old) but with "high" senescence (14.8%) is shown in Figure 1A. "Low" senescent CDCs from the aged donor were highly proliferative, with a higher proportion of Ki-67+ cells, and with a higher ability for wound closure compared to the "highly" senescent CDCs from the young donor.

No correlation was observed between chronological age and CDC senescence (Figure 1B). Donor chronological age did not influence CDC proliferative capacity (Population Doubling Time, PDT) nor DNA synthesis ($R^2 < 0.15$, $p > 0.1$), but it negatively affected CDC migration ($R^2 = 0.33$, $p < 0.05$, Figure 1B). In contrast to chronological age, EDCs senescence correlated to the gene expression of some aging-associated genes (i.e., *CDK2A* with $R^2 = 0.22$, $p < 0.05$, data not shown), and CDC senescence to most CDCs properties: CDC proliferation (PDT, $R^2 = 0.35$, $p < 0.05$), DNA synthesis ($R^2 = 0.34$, $p < 0.05$), and migration ($R^2 = 0.59$, $p < 0.001$) as shown in Figure 1C.

The chronological age or sex of the 34 human donors of cardiac tissue in our study have shown to be unrelated to molecular markers of cellular aging in EDCs derived from tissue samples under the same conditions (Figure S1). The chronological age did not correlate either to EDC senescence, to the gene expression of *CDKN1A*, *CDK2A*, and *TP53* in EDCs, or any of the other genes explored ($R^2 < 0.15$, $p > 0.1$, Figure S1). Chronological age did not correlate either to CDC telomere length or Vascular Endothelial Growth Factor (VEGF) secretion ($R^2 < 0.15$, $p > 0.1$, Figure S2).

Scoring the anti-aging potency of CDC-EVs *in vitro*

The obtained CDC-EVs were characterized in terms of their bioactivity using an aging-reversal potency matrix assay. In particular, the rejuvenating and pro-angiogenic potency was tested *in vitro* on EDCs (cardiac stromal cells, CSCs) previously obtained and human umbilical vein endothelial cells (HUVEC).

CDC-EVs were purified from CDCs obtained from 18 human donors and tested on CSCs from two human donors (target 1 with "moderate" basal senescence and target 2 with "high" basal senescence). The rejuvenating potency of CDC-EVs was determined by their ability to reduce CSC senescence, to induce CSC interleukin-6 (IL-6) secretion, and to reduce the gene expression of *CDKN1A* (p21), *CDKN2A* (p16), *TP53* (p53) *TGFB1* (TGF-β), and senescence and fibrosis-related genes in CSCs. CDC-EVs from different donors reduced senescence of target 1 between −3.2 and −8.1%. Similarly, in target 2, CSC senescence was reduced by all CDC-EVs as well (between −2.0 and −14.5%). However, the anti-senescent effect of the CDC-EVs did not correlate to any of the CDC characterization parameters explored (chronological age of the donors, cardiosphere size, percentage of senescent EDCs, or percentage of senescent CDCs). The relationship between EDC and CDC senescence and their derived CDC-EV anti-senescent effect is shown in Figure 2. The CDC-EV pro-angiogenic potency was determined by their ability to induce tube formation on HUVEC. Regarding angiogenic potential, all CDC-EVs except one, significantly improved endothelial branching length (between +15 and +58%). CDC-EVs pro-angiogenic effect did not correlate to their anti-senescent effect nor to any of the CDC characterization parameters explored ($R^2 < 0.15$, $p > 0.1$).

All CDC-EVs significantly increased CSC IL-6 secretion and most CDC-EVs reduced CSC *CDKN1A* and *CDKN2A* expression but only a few CDC-EVs reduced *TGFB1* and *TP53* expression in CSCs (Figure 3A).

Based on the individual results obtained for the 7 aging-related parameters evaluated in the assay, the total potency score was calculated for each CDC-EVs from different donors which were then classified as more-potent (green, total score between 11 and 14), mild potent (white, total score between 7.5 and 8.5), and less potent (red, between 5 and 7) (Figure 3B) using the matrix assay designed (Table S1). The CDC-EVs with the highest potency (1 and 2, with 14 and 12.5 points, respectively, in the potency score over max. 18 possible), were among the 33% CDC-EVs with the "best" results in most of the tests evaluated in the assay matrix. On the other hand, the least potent donor (18, with 5 points in the potency score), was among the "worst" 33% CDC-EVs in most of the potency tests in the assay matrix, not having shown a significant beneficial effect in most of the *in vitro* tests. The performance of each of the different CDC-EVs on the different parameters of the potency matrix assay is shown in Figure 3A. The chronological age of the donors did not correlate to the antiaging potency score of the CDC-EVs (Figure 3C). The pathology of each of the donors according to their position in the potency assay is detailed in Table S2.

According to these results, CDC-EVs from donors 1 (14-years old, male) and 2 (77-years old, female) were selected as the more-potent and used for treating animals assigned to the potent EVs group (P-EVs) *in vivo*. CDC-EVs from donor 18 (73 years old, male) were considered as the least-potent and were used for treating the animals assigned to the non-potent EVs group (NP-EVs). Performance of the P-EVs (donor 2) and NP-EVs (donor 18) vs. control conditions (serum free media alone, SFM) in some potency tests in the assay are shown in Figure 4. Both P-EVs and NP-EVs reduced senescence of CSCs of target 2, but P-EVs did it to a significantly larger extent ($n = 1520 \pm 18$ cells/condition). Relative tube formation in endothelial cells (HUVEC) under the effect of P-EVs ($n = 19 \pm 1$ images/condition) significantly increased, while it kept similar (slightly reduced, difference not significant) under the effect of NP-EVs.

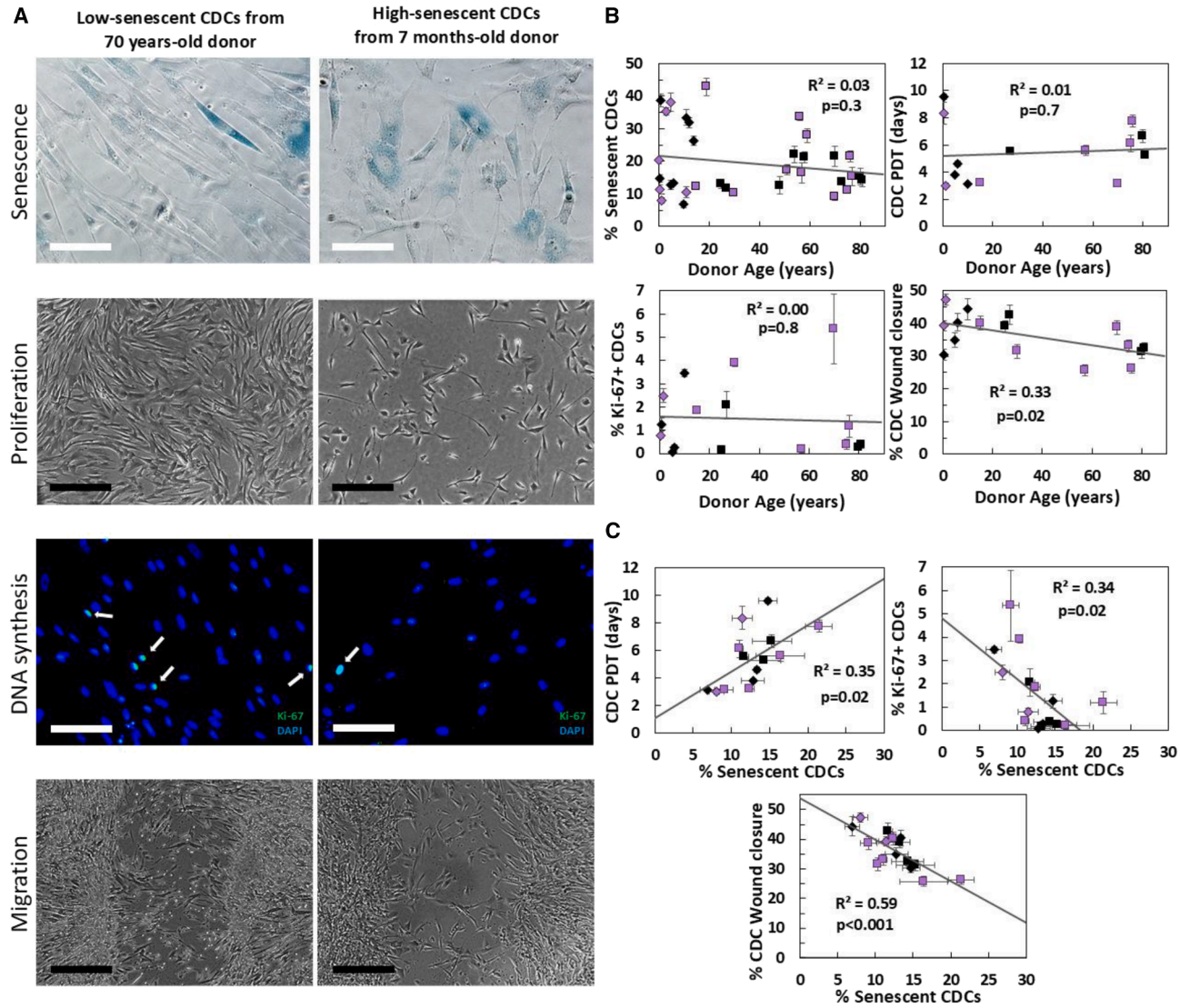

Figure 1. Donor chronological age vs. CDC biological age effect on different CDC properties

(A) Representative images from one chronologically aged donor (70-years old), but biologically young (9.1% of senescent CDCs) vs. one chronologically young donor (7-months old), but biologically aged (14.8% of senescent CDCs) after 72 h of culture.

(B) Chronological age is not significantly related to CDC senescence ($n = 34$ donors), population doubling time (PDT, $n = 14$), or DNA synthesis capacity (% Ki-67+ CDCs, $n = 16$) after 72 h of culture. Chronological age significantly affects CDC migration capacity after 24 h of wound generation (n = 16).

(C) CDC senescence however relates to PDT ($n = 14$), DNA synthesis ($n = 16$), and migration capacity ($n = 16$) significantly and to a higher extent. Adult samples are represented with a square, while pediatric samples are represented with a diamond. Male samples are shown in black and female samples in purple. White scale bar corresponds to 100 μm, black scale bar to 400 μm. p values obtained with t test.

Data are represented as mean ± SEM.

Validation of the *in vitro* aging-reversal potency assay in a rat model of premature cardiac senescence

More- and less-potent CDC-EVs selected according to their potency score in the matrix assay were tested in an *in vivo* model of premature cardiac aging (Figure 5A). Administration of daily D-galactose (D-gal) to rats had been demonstrated to induce cardiac-aging.[30] In our study, senescence of the cardiac tissue, measured by the expression of the *GLB1* gene, was significantly increased in rats with the daily administration of D-gal during 20 weeks (1.56 ± 0.17 vs. 1.00 ± 0.1 in the control group, $p < 0.05$) as shown in Figure 5B. Treatment with P-EVs abrogated the D-gal-induced aging, since the relative *GLB1* expression in P-EV-rats was significantly lower vs. the D-gal group (0.93 ± 0.19, $p < 0.05$) and similar to healthy controls. The use of NP-EVs showed only a non-significant trend for improvement.

Cardiac hypertrophy, measured as the ratio of the heart to the body weight, was barely increased by daily administration of D-gal in the whole group of animals (2.6 ± 0.09 vs. 2.5 ± 0.1 mg/g in the control group, Figure 5C) although the effect was more notorious in males (2.5 ± 0.05 vs. 2.2 ± 0.1 mg/g,

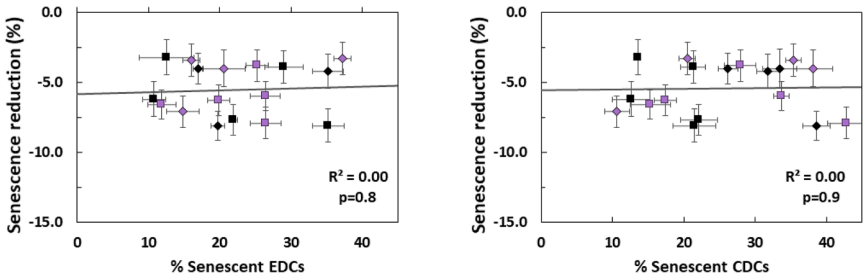

Figure 2. Correlation between EDC senescence (*n*= 17 donors) and CDC senescence (*n* = 18) vs. derived CDC-EVs anti-senescent potency in one of the CSC target donors (*n* = 1199 ± 27 cells/donor)

Adult samples are represented with a square, while pediatric samples are represented with a diamond. Male samples are shown in black and female samples in purple. *p* values obtained with t test. Data are represented as mean ± SEM.

$p < 0.01$; in D-gal vs. controls respectively). Given the absence of hypertrophy with D-gal, there was no room for further improvement using P-EVs. However, rats treated with NP-EVs developed cardiac hypertrophy (2.9 ± 0.11 mg/g) with $p < 0.05$ both vs. the healthy and the P-EVs groups. When considering only males, this difference was also significant vs. the D-gal group ($p < 0.05$).

Cardiac fibrosis was increased in D-gal rats (Figures 5D and 5E). At genetic level, administration of EVs prevented from significant increase in *TGFB1* relative expression observed in D-gal group (1.8 ± 0.2, $p = 0.01$ vs. healthy rats). Relative *TGFB1* expression was 1.6 ± 0.3 in the group receiving NP-EVs and 1.5 ± 0.23 with P-EVs, although the difference between both was not significant. Histological evaluation showed that interstitial fibrosis was significantly increased by D-gal administration (from 1.4 ± 0.2 to 2.0 ± 0.1%, $p < 0.05$) and in the D-gal rats treated with NP-EVs (2.1 ± 0.1%, $p < 0.05$ vs. healthy). The increase of the fibrosis in rats receiving D-gal but treated with P-EVs was not significant (2.0 ± 0.2%, $p > 0.05$). Representative images of cardiac fibrosis in animals in the different groups are shown in Figure 5E.

At functional level, D-gal administration did not affect cardiac perfusion. Cardiac perfusion measured by single photon emission computer tomography (SPECT) mean activity at the endpoint was similar in the healthy, D-gal, and D-gal + P-EVs groups (262 ± 7, 264 ± 13, and 252 ± 12 cps, respectively, all differences not significant, $p > 0.05$, Figure 5F). Nevertheless, cardiac perfusion of animals treated with NP-EVs was considerably worse than in animals in healthy and D-gal groups (220 ± 7 cps, $p < 0.05$ vs. healthy and D-gal). Representative images of SPECT activity in animals in all groups at endpoint are shown in Figure 5F. In a randomly selected subgroup of P-EV ($n = 4$) and NP-EV ($n = 2$) animals, SPECT was also performed at week-12, before the treatment was administered, showing an opposite trend in the perfusion evolution from week-12 to the endpoint in both groups (Figure S3). Serum levels of inflammaging-related tumor necrosis factor alpha (TNF-α) and IL-6 were increased in D-gal rats and were lower in EV-treated animal, with a slightly better profile in P-EV vs. NP-EV groups (Figure 6).

DISCUSSION

A simple *in vitro* assay proposed in this study permits to select therapeutically more potent CDC-EVs to reverse cardiac aging in a living organism. The rejuvenating potency of CDC-EVs in our study was determined in a step-forward approach, by their ability to favorably modulate six senescence-related genetic, protein and bioactivity markers gathered in a matrix assay. Markers selected in the assay are linked to the potential MoA by which CDC-EVs are expected to exert their beneficial effects in the treatment of cardiac aging.[31–37]

The lack of suitable *in vitro* assays to monitor the therapeutic potential of EVs currently restricts their application in clinical studies. Although challenging because of the complexity of the MoA of native EVs, testing their biological activity by using a potency test *in vitro* or *in vivo* is recommended by expert working groups in the field.[21,38] These assays will ensure that only EV-products of consistent potency are released for clinical testing or therapeutic use. In fact, as our results show, some of the EVs may even have negative effects contributing to the controversial or neutral results observed in other studies.[11,16,39–43] Thus, development of potency tests will promote rigorous, robust clinical testing of EV-based drug products and accelerate clinical translation. As suggested previously,[24] in this study, we designed the potency test considering the anti-senescent effect of the CDC-EVs as the most relevant MoA to counteract the aging-related cardiac changes underlying some types of HFpEF. The reduction of the senescence in different cardiac cell types, as well as stimulating angiogenesis has been associated to multiple therapeutical benefits in cardiac aging.[44–47]

Our results show that EVs classified as potent (P-EVs) with the *in vitro* matrix assay had higher cardiac rejuvenating potency *in vivo* than EVs classified as non-potent (NP-EVs). While P-EVs had the potential to significantly reduce the expression of the senescence-associated gene *GLB1* in D-gal age-induced-animals and to non-significantly reduce cardiac hypertrophy and *TGFB1* expression, NP-EVs did not significantly produce any effect and in fact significantly increased cardiac hypertrophy, cardiac fibrosis, and reduced perfusion. These results are in accordance with the effects observed in the *in vitro* functional assay. While P-EVs (from donors 1 and 2) had significant beneficial effects in most *in vitro* effects explored (reducing CSC senescence, increasing CSC IL-6 secretion, reducing the genetic expression of senescence-associated genes, and improving angiogenesis), NP-EVs (from donor 18) only significantly improved CSC senescence in one of the two target donors, increased CSC IL-6 secretion, and reduced *CDKN2A* expression. In addition, NP-EVs *in vitro* even tended to increase *TGFB1*, *TP53*, and *CDKN2A* expression in CSCs and reduced endothelial tube formation. These results highlight the importance of human CDC-EV variation in modulating target cellular responses and confirm that their effects can be positive, absent

A

			Effect of CDC-EVs on CSCs from Target 1						Effect of CDC-EVs on CSCs from Target 2						Effect of CDC-EVs on HUVEC
Donor	Age	Gender	Senescence reduction (%)	IL-6 (pg/ml)	*CDKN1A*	*CDKN2A*	*TP53*	*TGFB1*	Senescence reduction (%)	IL-6 (pg/ml)	*CDKN1A*	*CDKN2A*	*TP53*	*TFGB1*	Relative tube formation
1	14 y	M	-4.0	211	0.04	0.00	0.65	0.60	-9.0	170	0.79	1.03	0.54	0.53	1.51
2	77 y	F	-6.6	165	0.65	0.52	1.22	0.82	-11.9	73	0.85	0.69	1.12	0.75	1.56
3	51 y	F	-6.3	312	1.10	0.28	0.88	0.92	-6.7	238	0.80	0.79	0.90	0.88	1.41
4	59 y	F	-3.8	207	0.48	0.46	0.77	0.83	-9.8	203	0.68	0.85	1.31	1.00	1.32
5	8 m	M	-8.1	127	0.01	0.48	1.92	1.26	-11.0	128	0.85	0.87	1.42	0.84	1.46
6	70 y	M	-8.1	77	0.36	0.07	0.09	0.14	-2.0	117	0.57	1.21	1.72	0.79	1.32
7	58 y	M	-3.9	143	0.24	0.10	1.38	1.00	-14.2	76	0.41		0.93	0.56	1.25
8	11 y	F	-7.1	71	0.53	0.30	0.99	0.58	-6.3	90	1.32	1.02	1.05	0.82	1.15
9	5 y	F	-4.0	108	0.78	0.26	1.37	0.99	-14.5	160	0.01	1.92	1.91	1.00	1.43
10	19 y	F	-7.9	68	0.35	0.12	0.67	1.06	-4.9	41	1.20	1.23	1.15	0.89	1.51
11	12 y	M	-4.2	77	0.66	0.36	1.24	1.06	-10.0	96	1.03	1.36	1.69	0.95	1.58
12	48 y	M	-6.2	227	0.39	0.43	1.16	1.29	-7.4	230	1.39	1.12	1.71	0.95	1.27
13	3 m	F	-3.3	136	0.62	0.35	1.27	1.27	-5.5	87	1.35	0.77	0.93	0.89	1.32
14	3 y	F	-3.4	72	0.35	0.21	0.73	1.00	-8.4	29	0.94	0.68	0.87	0.77	1.25
15	54 y	M	-7.7		0.69	0.15	2.12	1.29	-3.0	98	1.47	1.25	1.64	0.76	1.33
16	11 y	M	-4.0	48	0.48	0.28	0.98	0.87	-3.2	160	0.82	0.83	2.06	1.01	1.33
17	56 y	F	-6.0	70	0.44	0.17	1.51	1.44	-3.9		0.62	0.00	1.88	0.49	1.31
18	73 y	M	-3.2	112	0.69	0.44	1.76	1.61	-6.9	70	0.37	2.23	0.78	0.67	0.94

B

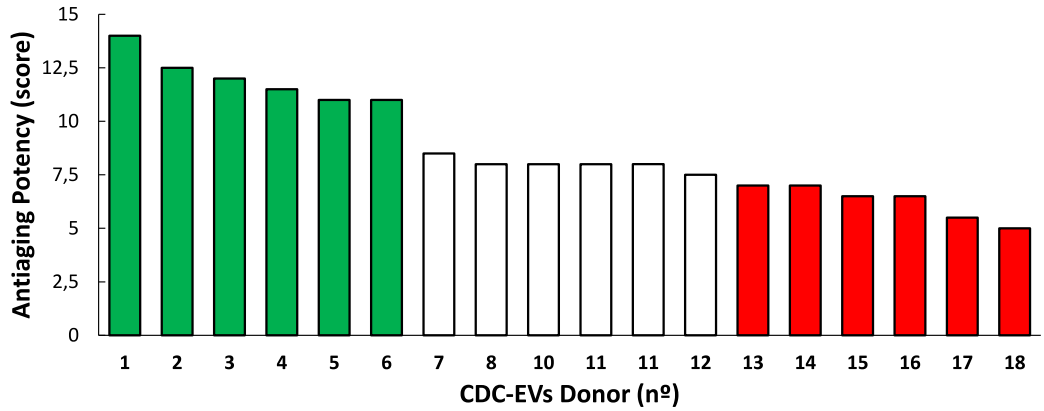

C

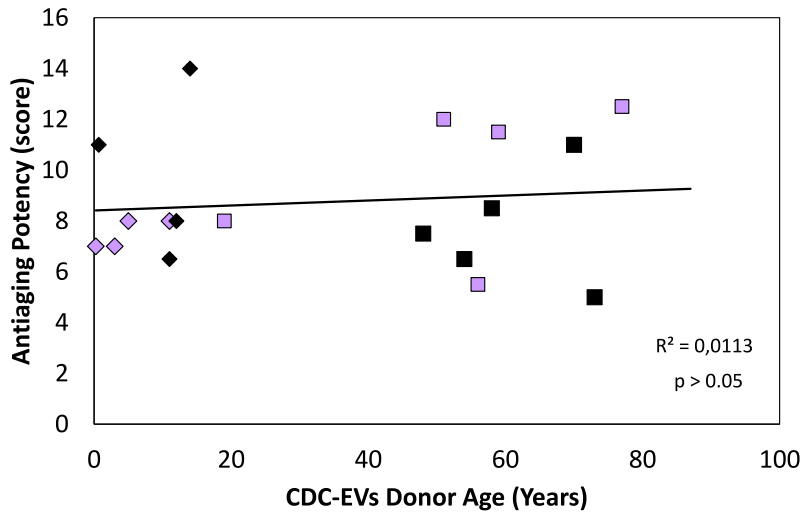

(legend on next page)

or even negative in some cases and that *in vitro* potency tests can serve as *in vivo* predictors to identify optimal and discardable products for expected specific MoA.

Clinical trials in patients with HFpEF have been failing to demonstrate robust efficacy of different pharmacological strategies during decades until recently, when two drugs from the group of sodium-glucose cotransporter type 2 inhibitors proved to meaningfully reduce the HF hospitalizations and cardiovascular death.[48] However, because of the increasing prevalence of the HFpEF, with high morbidity and mortality rates, this syndrome still constitutes an important target for the new drug-development research.

In light of the increasing awareness for treatments in patients with HFpEF, the development of corresponding animal models would be highly desired.[49] There is increasing evidence that the chronic exposure to D-gal in rodents is associated to an enhanced cardiac expression of senescence markers, oxidative stress, inflammation, mitochondrial dysfunction, fibrosis, and hypertrophy that ultimately are translated into diastolic dysfunction[30,50,51] observed in aging-related HFpEF. By using the D-gal model of accelerated aging in our study, we could reproduce some of the previously described effects on cardiac tissue such as an increased senescence and fibrosis and higher serum levels of inflammatory markers. However, despite using a higher dose compared to previous publications, our study failed to demonstrate an increase in cardiac hypertrophy in the global group (it was only reproduced in males) and changes in parameters of diastolic dysfunction, such as end-diastolic pressure, min dP/dT, or Tau (data not shown). In terms of cardiac fibrosis, it is worthy to note that even if increased in D-gal rats compared to healthy controls, it was meaningfully lower (2% vs. ~8% or higher) than that reported in other studies where CDCs and CDC-EVs showed rejuvenating effects.[10] In general, in this study D-gal administration only induced moderate changes at cardiac level. Small changes were observed in *GLB1* expression, hypertrophy and cardiac fibrosis compared to healthy animals not receiving D-gal. Therefore, as D-gal administration did not seem to induce large damage at cellular, structural, and functional level, this probably gave little room for the P-EVs to exert more significant benefits. All these considerations are important to take into account while interpreting at some extent only modest beneficial effects of the P-EVs in our D-gal animals.

In conclusion, if confirmed in other aging-related disease animal models, the matrix assay proposed here could be a suitable *in vitro* potency test for discerning suitable EVs for their allogenic use in clinical trials of aging related HF-pEF.

Limitations of the study

Several limitations of our study need to be considered. As mentioned before, the rat model of D-gal-induced premature aging we used in the study did not recapitulate all the cardiac changes, especially those related with diastolic dysfunction, described previously.[52–55] This might have affected mostly the potentially beneficial effects of the P-EVs. However, we did confirm our hypothesis by demonstrating a more favorable therapeutic profile of the P-EVs vs. NP-EVs in other genetic and structural parameters where the model worked appropriately, although the degree of these changes was still far from the described in naturally aged animals.[11,56–58] On the other hand, although the number of human donors included in our study was not small (n = 18) and the chronological age range was wide (3 months–81 years old), larger sample size, and inclusion of neonate samples, would permit to make a more robust conclusion about the implication of the chronological age of the donors on the potency of the therapeutic product, absent in this study. A larger sample size would also help define pass and fail quantitative ranges for the therapeutic EVs instead of qualitative ones used in this study.

Finally, all tissue samples were obtained from sick donors who underwent cardiac surgery for different reasons. As this could have affected some of the characteristics of the derived cells, the inclusion of healthy donors would be of interest for the purpose of the study. However, even among the adult group where the disease type and the progression of the disease was uniform (mitral valve insufficiency), we did not observe a relationship between the chronological age, CDC senescence, or antiaging *in vitro* performance. Interestingly, the CDC-EVs derived from an adult that was additionally suffering from multivessel coronary artery disease were the ones presenting the least potency score, classified as NP and even showing some deleterious effects in both the *in vitro* assay and the *in vivo* experiments.

In spite of all the limitations, the results highlight the importance of performing adequate potency tests before using biological products in the clinical scenario, as the use of non-potent or

Figure 3. CDC-EV potency assay results for the different donors

(A) Characterization and performance of CDC-EVs from the different donors in the different tests in the potency matrix assay. The values in the table indicate donor position according to results in the potency test, age, gender, and performance in each of the different tests in the potency assay matrix. Reduction in cardiac stroma cell (CSC) senescence (in two target donors) induced by the different CDC-EVs (n = 1199 ± 27 cells/condition in target donor 1 and n = 1520 ± 18 cells/condition in target donor 2). Increment in CSC IL-6 secretion vs. serum-free media (SFM) alone (in two target donors) induced by the different CDC-EVs (n = 3 samples/condition). *CDKN1A*, *CDKN2A*, *TP53*, and *TGFB1* relative expression in CSC (from two target donors) under the effect of the different CDC-EVs (n = 3 samples/condition). Relative tube formation in endothelial cells (HUVEC) under the effect of the different CDC-EVs (n = 19 ± 1 images/condition). All data are with respect to untreated CSCs or endothelial cells under SFM. Values in green indicate the donors that showed the most effect in the corresponding test (belonged to the best tercile) and therefore received the maximum score in that particular test. Values in red indicate the donors that showed the least beneficial effect in the corresponding test (belonged to the worst tercile) and therefore received a 0 score in that particular test.

(B) Total score obtained in the potency matrix assay, used for the classification of potent CDC-EVs, mild-potent CDC-EVs and non-potent CDC-EVs. Donors in green presented the highest total antiaging potency score (belonged to the best tercile) and were classified as potent (P-EVs). Donors in red presented the lowest total antiaging potency score (belonged to the worst tercile) and were classified as non-potent (NP-EVs).

(C) Correlation between the age of the donor and the anti-aging potency score of the derived CDC-EV (n = 18). p value obtained with t test. A, adult; P, pediatric; M, male; F, female; Y, years; m, months.

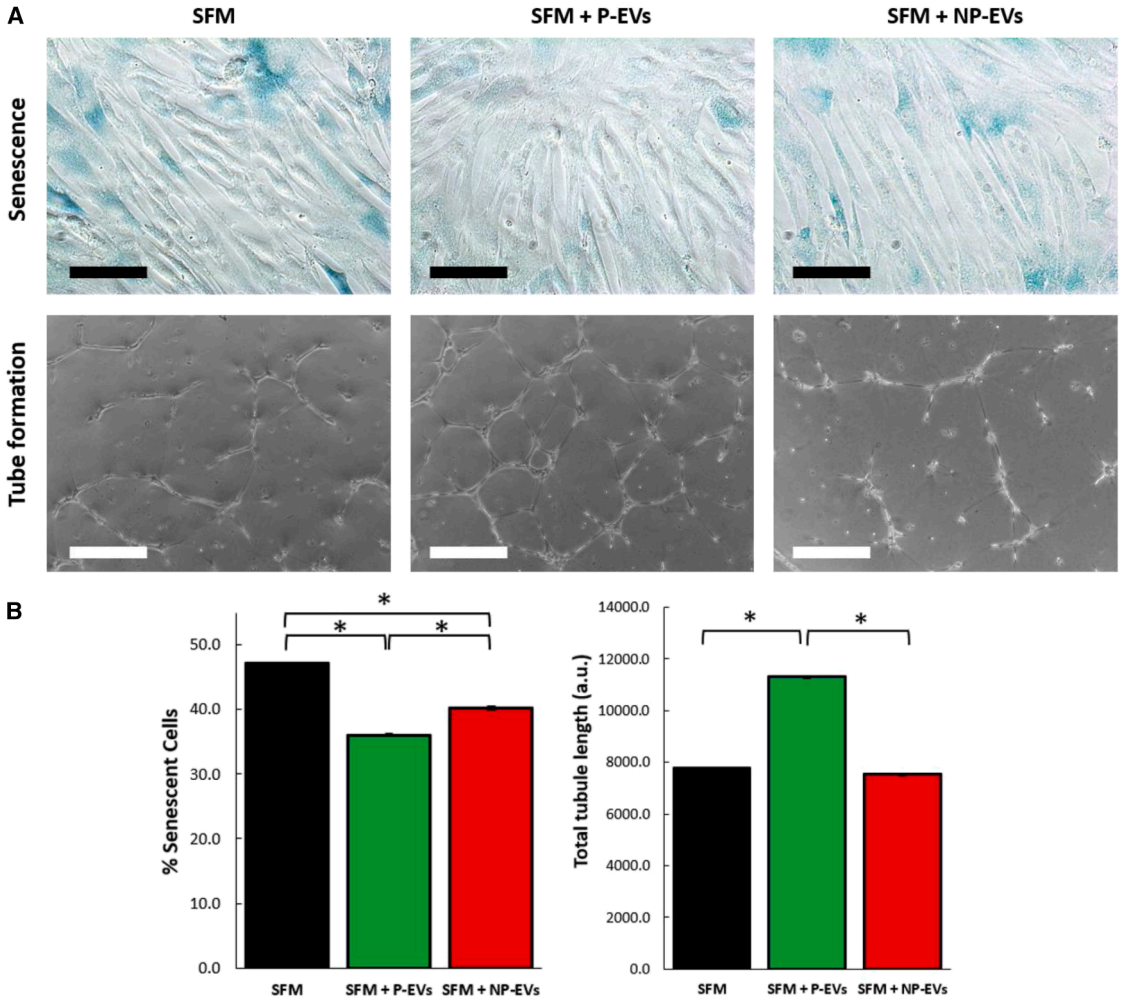

Figure 4. Performance of the P-EVs (donor 2) and NP-EVs (donor 18) vs. control conditions (SFM) in some potency tests in the assay

(A) Representative images from the senescence and the tube formation test under control conditions, P-EVs and NP-EVs.

(B) Both P-EVs and NP-EVs reduced senescence of CSCs of target 2, but P-EVs did it to a significantly larger extent (n = 1520 ± 18 cells/condition). Relative tube formation in endothelial cells (HUVEC) under the effect of P-EVs (n = 19 ± 1 images/condition) significantly increased, while it kept similar (slightly reduced, difference not significant) under the effect of NP-EVs. P, potent; NP, non-potent; SFM, serum free media. *$p < 0.05$. Black scale bar corresponds to 100 μm, white scale bar to 400 μm. p values obtained with t test.

Data are represented as mean ± SEM.

suboptimal products may lead to unforeseen results and lack of desired efficacy.

RESOURCE AVAILABILITY

Lead contact

Further information and requests for resources should be directed to and will be fulfilled by the lead contact, Grigorian-Shamagian Lilian (grigorianl@yahoo.es).

Materials availability

This study did not generate new unique reagents. The reagents and materials used and their accession codes can be found in the key resources table.

Data and code availability

- Data: The data supporting the findings of this study are available within the paper and its supplementary information files. Additional data are available from the corresponding author upon request.
- Code: Previously published software and codes used to analyze the results (ImageJ) are referenced in the key resources table.
- Other: Any additional information required to reanalyze the data reported in this paper is available from the lead contact upon reasonable request.

ACKNOWLEDGMENTS

This research was funded by the Instituto de Salud Carlos III, Ministerio de Ciencia e Innovación, Spain: PI16/01123; PI19/00161; PI22.00792; Red de Terapia Celular, Tercel, (RD16.0011.0029) and CIBERCV (CB16.11.00292).

AUTHOR CONTRIBUTIONS

G.-C.L. processed the biopsies, performed the experiments, analyzed and interpreted the data, prepared the figures and drafted the manuscript. C.-N.M., C.-F.A., O.A., and S.S.-S. provided technical assistance. P.A. and G.-J.J.M. contributed to sample collection. F.-A.F. acquired the funding, supervised

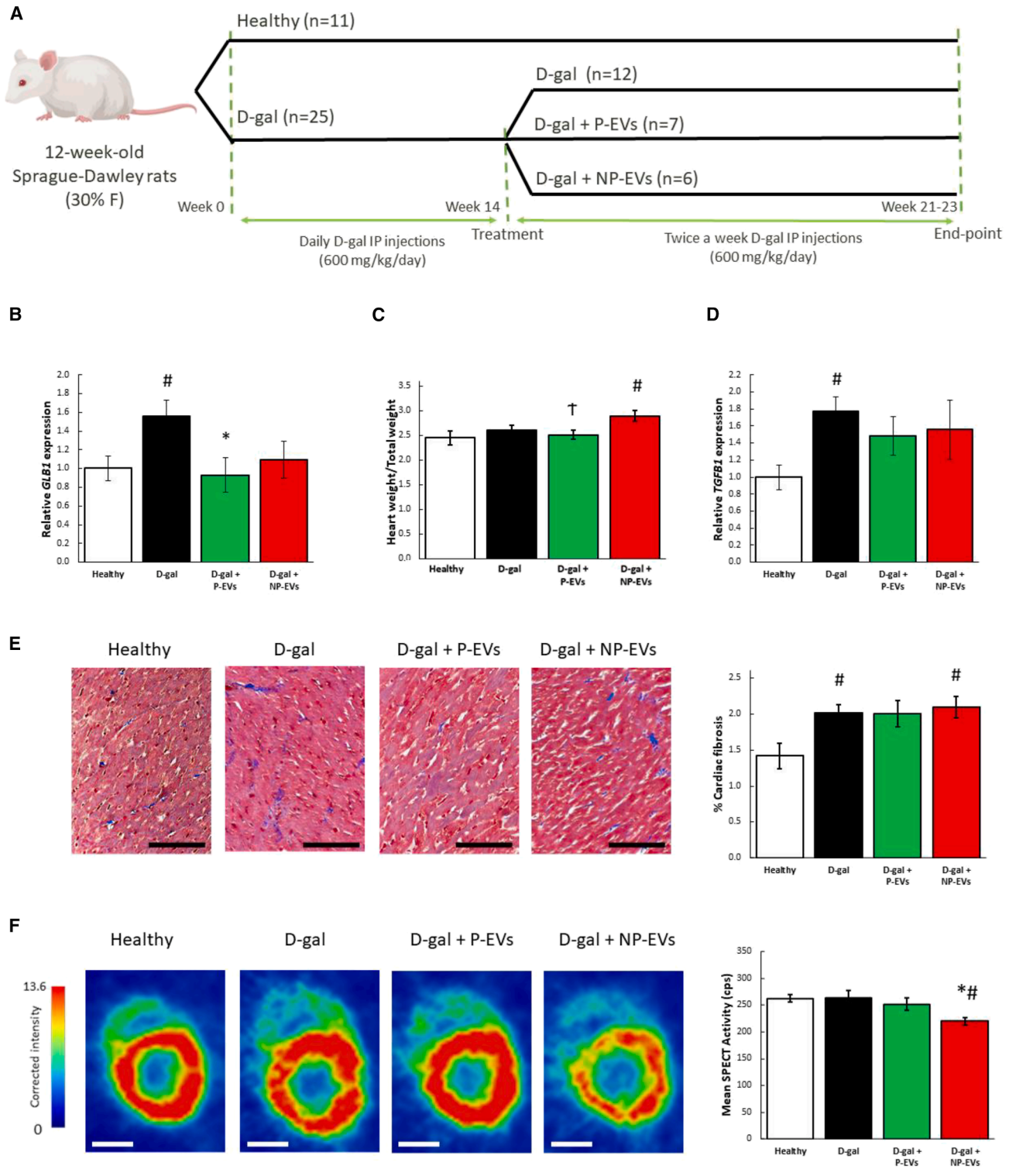

Figure 5. Cardiac effects of D-gal and P- and NP-EV administration

(A) P-EVs and NP-EVs rejuvenating and pro-angiogenic potency was tested in a rodent model of cardiac aging. Timeline including group distribution, product administration and tests performed.

(B) Effects on cardiac senescence at genetic level (Healthy: *n* = 6, D-gal: *n* = 11, D-gal + P-EVs: *n* = 7, D-gal + NP-EVs: *n* = 6).

(C) Effects on cardiac hypertrophy on the whole population (Healthy: *n* = 8, D-gal: *n* = 12, D-gal + P-EVs: *n* = 7, D-gal + NP-EVs: *n* = 6).

(legend continued on next page)

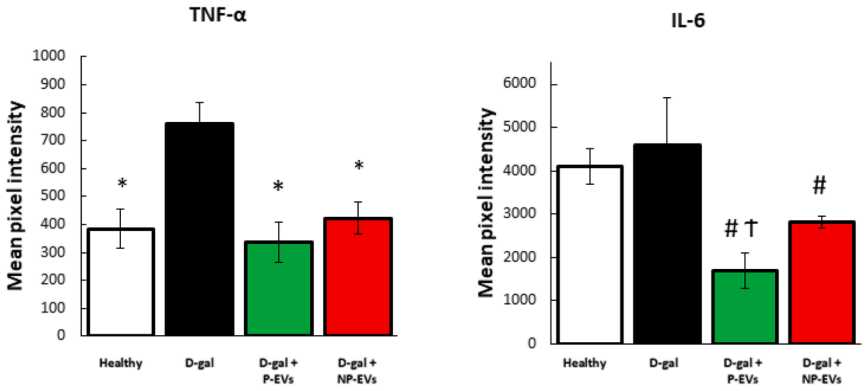

Figure 6. Effect of of D-gal and P- and NP-EV administration in TNF-α and IL-6 levels in peripheral blood (Healthy: *n* = 4, D-gal: *n* = 4, D-gal + P-EVs: *n* = 4, D-gal + NP-EVs: *n* = 4)

D-gal, D-galactose; EVs, extracellular vesicles; P, potent; NP, non-potent. *$p < 0.05$ vs. D-gal, #$p < 0.05$ vs. Healthy, † $p < 0.05$ vs. NP-EVs in Student t test. Data are represented as mean ± SEM.

the project and critically revised the work. G.-S.L. designed, supervised, validated the work and helped draft the manuscript. All authors read and approved the final manuscript.

DECLARATION OF INTERESTS

The authors declare no competing interests.

STAR★METHODS

Detailed methods are provided in the online version of this paper and include the following:

- KEY RESOURCES TABLE
- EXPERIMENTAL MODEL AND SUBJECT DETAILS
  - Cardiac biopsies from human subjects
  - Generation of EDCs and CDCs
  - Animal models
- METHOD DETAILS
  - Cell culture
  - Generation and characterization of CDC-EVs
  - Characterization of EDCs and CDCs
  - Design of the ageing-reversal potency matrix assay
  - *In vivo* evaluation
- QUANTIFICATION AND STATISTICAL ANALYSIS
- ADDITIONAL RESOURCES

SUPPLEMENTAL INFORMATION

Supplemental information can be found online at https://doi.org/10.1016/j.isci.2025.112910.

Received: January 10, 2025
Revised: April 9, 2025
Accepted: June 12, 2025
Published: June 16, 2025

REFERENCES

1. Steenman, M., and Lande, G. (2017). Cardiac aging and heart disease in humans. Biophys. Rev. *9*, 131–137. https://doi.org/10.1007/s12551-017-0255-9.
2. Borlaug, B.A. (2020). Evaluation and management of heart failure with preserved ejection fraction. Nat. Rev. Cardiol. *17*, 559–573. https://doi.org/10.1038/s41569-020-0363-2.
3. Redfield, M.M., and Borlaug, B.A. (2023). Heart Failure With Preserved Ejection Fraction: A Review. JAMA *329*, 827–838. https://doi.org/10.1001/jama.2023.2020.
4. Abdellatif, M., Rainer, P.P., Sedej, S., and Kroemer, G. (2023). Hallmarks of cardiovascular ageing. Nat. Rev. Cardiol. *20*, 754–777. https://doi.org/10.1038/s41569-023-00881-3.
5. Climent, A.M., Sanz-Ruiz, R., and Fernández-Avilés, F. (2017). Cardiac rejuvenation: a new hope in the presbycardia nightmare. Eur. Heart J. *38*, 2968–2970. https://doi.org/10.1093/eurheartj/ehx498.
6. Yanai, H., and Fraifeld, V.E. (2018). The role of cellular senescence in aging through the prism of Koch-like criteria. Ageing Res. Rev. *41*, 18–33. https://doi.org/10.1016/j.arr.2017.10.004.
7. Uren, N.G., Camici, P.G., Melin, J.A., Bol, A., de Bruyne, B., Radvan, J., Olivotto, I., Rosen, S.D., Impallomeni, M., and Wijns, W. (1995). Effect of aging on myocardial perfusion reserve. J. Nucl. Med. *36*, 2032–2036.
8. Gazoti Debessa, C.R., Mesiano Maifrino, L.B., and Rodrigues de Souza, R. (2001). Age related changes of the collagen network of the human heart. Mech. Ageing Dev. *122*, 1049–1058. https://doi.org/10.1016/s0047-6374(01)00238-x.
9. Rudnitsky, E., Braiman, A., Wolfson, M., Muradian, K.K., Gorbunova, V., Turgeman, G., and Fraifeld, V.E. (2024). Stem cell-derived extracellular vesicles as senotherapeutics. Ageing Res. Rev. *99*, 102391. https://doi.org/10.1016/j.arr.2024.102391.
10. Grigorian Shamagian, L., Rogers, R.G., Luther, K., Angert, D., Echavez, A., Liu, W., Middleton, R., Antes, T., Valle, J., Fourier, M., et al. (2023). Rejuvenating effects of young extracellular vesicles in aged rats and in cellular models of human senescence. Sci. Rep. *13*, 12240. https://doi.org/10.1038/s41598-023-39370-5.
11. Grigorian-Shamagian, L., Liu, W., Fereydooni, S., Middleton, R.C., Valle, J., Cho, J.H., and Marbán, E. (2017). Cardiac and systemic rejuvenation

(D and E) (D) Effects on cardiac fibrosis at genetic (Healthy: *n* = 6, D-gal: *n* = 11, D-gal + P-EVs: *n* = 7, D-gal + NP-EVs: *n* = 6) and (E) tissue level (Healthy: *n* = 4, D-gal: *n* = 12, D-gal + P-EVs: *n* = 7, D-gal + NP-EVs: *n* = 6). Representative images of interstitial fibrosis in animals in each group.
(F) Effects on cardiac perfusion (Healthy: *n* = 4, D-gal: *n* = 4, D-gal + P-EVs: *n* = 6, D-gal + NP-EVs: *n* = 4). Representative images of single photon emission computer tomography (SPECT) intensity corrected by injected activity, animal weight, and acquisition time in animals in the different groups. F, female; D-gal, D-galactose; EVs, extracellular vesicles; P, potent; NP, non-potent. *$p < 0.05$ vs. D-gal, #$p < 0.05$ vs. Healthy, † $p < 0.05$ vs. NP-EVs in Student t test. Black scale bar corresponds to 100 μm. White scale bar corresponds to 5 mm.
Data are represented as mean ± SEM.

after cardiosphere-derived cell therapy in senescent rats. Eur. Heart J. *38*, 2957–2967. https://doi.org/10.1093/eurheartj/ehx454.

12. Malliaras, K., Ibrahim, A., Tseliou, E., Liu, W., Sun, B., Middleton, R.C., Seinfeld, J., Wang, L., Sharifi, B.G., and Marbán, E. (2014). Stimulation of endogenous cardioblasts by exogenous cell therapy after myocardial infarction. EMBO Mol. Med. *6*, 760–777. https://doi.org/10.1002/emmm.201303626.

13. Tseliou, E., de Couto, G., Terrovitis, J., Sun, B., Weixin, L., Marbán, L., and Marbán, E. (2014). Angiogenesis, cardiomyocyte proliferation and anti-fibrotic effects underlie structural preservation post-infarction by intramyocardially-injected cardiospheres. PLoS One *9*, e88590. https://doi.org/10.1371/journal.pone.0088590.

14. Chimenti, I., Smith, R.R., Li, T.-S., Gerstenblith, G., Messina, E., Giacomello, A., and Marbán, E. (2010). Relative roles of direct regeneration versus paracrine effects of human cardiosphere-derived cells transplanted into infarcted mice. Circ. Res. *106*, 971–980. https://doi.org/10.1161/CIRCRESAHA.109.210682.

15. López, E., Marinaro, F., de Pedro, M.d.L.Á., Sánchez-Margallo, F.M., Gómez-Serrano, M., Ponath, V., Pogge von Strandmann, E., Jorge, I., Vázquez, J., Fernández-Pereira, L.M., et al. (2020). The Immunomodulatory Signature of Extracellular Vesicles From Cardiosphere-Derived Cells: A Proteomic and miRNA Profiling. Front. Cell Dev. Biol. *8*, 321. https://doi.org/10.3389/fcell.2020.00321.

16. Smith, R.R., Barile, L., Cho, H.C., Leppo, M.K., Hare, J.M., Messina, E., Giacomello, A., Abraham, M.R., and Marbán, E. (2007). Regenerative potential of cardiosphere-derived cells expanded from percutaneous endomyocardial biopsy specimens. Circulation *115*, 896–908. https://doi.org/10.1161/CIRCULATIONAHA.106.655209.

17. Davis, D.R., Zhang, Y., Smith, R.R., Cheng, K., Terrovitis, J., Malliaras, K., Li, T.-S., White, A., Makkar, R., and Marbán, E. (2009). Validation of the cardiosphere method to culture cardiac progenitor cells from myocardial tissue. PLoS One *4*, e7195. https://doi.org/10.1371/journal.pone.0007195.

18. Ishigami, S., Ohtsuki, S., Eitoku, T., Ousaka, D., Kondo, M., Kurita, Y., Hirai, K., Fukushima, Y., Baba, K., Goto, T., et al. (2017). Intracoronary cardiac progenitor cells in single ventricle physiology: The PERSEUS (Cardiac Progenitor Cell Infusion to Treat Univentricular Heart Disease) Randomized Phase 2 Trial. Circ. Res. *120*, 1162–1173. https://doi.org/10.1161/CIRCRESAHA.116.310253.

19. Makkar, R.R., Kereiakes, D.J., Aguirre, F., Kowalchuk, G., Chakravarty, T., Malliaras, K., Francis, G.S., Povsic, T.J., Schatz, R., Traverse, J.H., et al. (2020). Intracoronary ALLogeneic heart STem cells to Achieve myocardial Regeneration (ALLSTAR): a randomized, placebo-controlled, double-blinded trial. Eur. Heart J. *41*, 3451–3458. https://doi.org/10.1093/eurheartj/ehaa541.

20. McDonald, C.M., Marbán, E., Hendrix, S., Hogan, N., Ruckdeschel Smith, R., Eagle, M., Finkel, R.S., Tian, C., Janas, J., Harmelink, M.M., et al. (2022). Repeated intravenous cardiosphere-derived cell therapy in late-stage Duchenne muscular dystrophy (HOPE-2): a multicentre, randomised, double-blind, placebo-controlled, phase 2 trial. Lancet *399*, 1049–1058. https://doi.org/10.1016/S0140-6736(22)00012-5.

21. Grigorian-Shamagian, L., Sanz-Ruiz, R., Climent, A., Badimon, L., Barile, L., Bolli, R., Chamuleau, S., Grobbee, D.E., Janssens, S., Kastrup, J., et al. (2021). Insights into therapeutic products, preclinical research models, and clinical trials in cardiac regenerative and reparative medicine: where are we now and the way ahead. Current opinion paper of the ESC Working Group on Cardiovascular Regenerative and Reparative Medicine. Cardiovasc. Res. *117*, 1428–1433. https://doi.org/10.1093/cvr/cvaa337.

22. Povsic, T.J., Sanz-Ruiz, R., Climent, A.M., Bolli, R., Taylor, D.A., Gersh, B.J., Menasché, P., Perin, E.C., Pompilio, G., Atsma, D.E., et al. (2021). Reparative cell therapy for the heart: critical internal appraisal of the field in response to recent controversies. ESC Heart Fail. *8*, 2306–2309. https://doi.org/10.1002/ehf2.13256.

23. Welsh, J.A., Goberdhan, D.C.I., O'Driscoll, L., Buzas, E.I., Blenkiron, C., Bussolati, B., Cai, H., Di Vizio, D., Driedonks, T.A.P., Erdbrügger, U., et al. (2024). Minimal information for studies of extracellular vesicles (MISEV2023): From basic to advanced approaches. J. Extracell. Vesicles *13*, e12404. https://doi.org/10.1002/jev2.12404.

24. Gómez-Cid, L., Grigorian-Shamagian, L., Sanz-Ruiz, R., de la Nava, A.S., Fernández, A.I., Fernández-Santos, M.E., and Fernández-Avilés, F. (2021). The essential need for a validated potency assay for cell-based therapies in cardiac regenerative and reparative medicine. a practical approach to test development. Stem Cell Rev. Rep. *17*, 2235–2244. https://doi.org/10.1007/s12015-021-10244-5.

25. Cheng, K., Malliaras, K., Smith, R.R., Shen, D., Sun, B., Blusztajn, A., Xie, Y., Ibrahim, A., Aminzadeh, M.A., Liu, W., et al. (2014). Human cardiosphere-derived cells from advanced heart failure patients exhibit augmented functional potency in myocardial repair. JACC Heart Fail. *2*, 49–61. https://doi.org/10.1016/j.jchf.2013.08.008.

26. Ibrahim, A.G.E., Li, C., Rogers, R., Fournier, M., Li, L., Vaturi, S.D., Antes, T., Sanchez, L., Akhmerov, A., Moseley, J.J., et al. (2019). Augmenting canonical Wnt signalling in therapeutically inert cells converts them into therapeutically potent exosome factories. Nat. Biomed. Eng. *3*, 695–705. https://doi.org/10.1038/s41551-019-0448-6.

27. Porat, Y., Abraham, E., Karnieli, O., Nahum, S., Woda, J., and Zylberberg, C. (2015). Critical elements in the development of cell therapy potency assays for ischemic conditions. Cytotherapy *17*, 817–831. https://doi.org/10.1016/j.jcyt.2014.08.014.

28. Willis, G.R., Kourembanas, S., and Mitsialis, S.A. (2017). Toward exosome-based therapeutics: isolation, heterogeneity, and fit-for-purpose potency. Front. Cardiovasc. Med. *4*, 63. https://doi.org/10.3389/fcvm.2017.00063.

29. Marbán, E. (2018). A mechanistic roadmap for the clinical application of cardiac cell therapies. Nat. Biomed. Eng. *2*, 353–361. https://doi.org/10.1038/s41551-018-0216-z.

30. Bo-Htay, C., Palee, S., Apaijai, N., Chattipakorn, S.C., and Chattipakorn, N. (2018). Effects of d-galactose-induced ageing on the heart and its potential interventions. J. Cell. Mol. Med. *22*, 1392–1410. https://doi.org/10.1111/jcmm.13472.

31. Valieva, Y., Ivanova, E., Fayzullin, A., Kurkov, A., and Igrunkova, A. (2022). Senescence-Associated β-Galactosidase Detection in Pathology. Diagnostics *12*, 2309. https://doi.org/10.3390/diagnostics12102309.

32. Scheller, J., Chalaris, A., Schmidt-Arras, D., and Rose-John, S. (2011). The pro- and anti-inflammatory properties of the cytokine interleukin-6. Biochim. Biophys. Acta *1813*, 878–888. https://doi.org/10.1016/j.bbamcr.2011.01.034.

33. Xing, Z., Gauldie, J., Cox, G., Baumann, H., Jordana, M., Lei, X.F., and Achong, M.K. (1998). IL-6 is an antiinflammatory cytokine required for controlling local or systemic acute inflammatory responses. J. Clin. Invest. *101*, 311–320.

34. López-Domínguez, J.A., Rodríguez-López, S., Ahumada-Castro, U., Desprez, P.-Y., Konovalenko, M., Laberge, R.-M., Cárdenas, C., Villalba, J.M., and Campisi, J. (2021). *Cdkn1a* transcript variant 2 is a marker of aging and cellular senescence. Aging *13*, 13380–13392. https://doi.org/10.18632/aging.203110.

35. He, S., and Sharpless, N.E. (2017). Senescence in Health and Disease. Cell *169*, 1000–1011. https://doi.org/10.1016/j.cell.2017.05.015.

36. Mijit, M., Caracciolo, V., Melillo, A., Amicarelli, F., and Giordano, A. (2020). Role of p53 in the Regulation of Cellular Senescence. Biomolecules *10*, 420. https://doi.org/10.3390/biom10030420.

37. Tominaga, K., and Suzuki, H.I. (2019). TGF-β signaling in cellular senescence and aging-related pathology. Int. J. Mol. Sci. *20*, 5002. https://doi.org/10.3390/ijms20205002.

38. Silva, A.K.A., Morille, M., Piffoux, M., Arumugam, S., Mauduit, P., Larghero, J., Bianchi, A., Aubertin, K., Blanc-Brude, O., Noël, D., et al. (2021). Development of extracellular vesicle-based medicinal products:

A position paper of the group "Extracellular Vesicle translatiOn to clinicaL perspectiVEs - EVOLVE France". Adv. Drug Deliv. Rev. *179*, 114001. https://doi.org/10.1016/j.addr.2021.114001.

39. Madonna, R., Van Laake, L.W., Davidson, S.M., Engel, F.B., Hausenloy, D. J., Lecour, S., Leor, J., Perrino, C., Schulz, R., Ytrehus, K., et al. (2016). Position Paper of the European Society of Cardiology Working Group Cellular Biology of the Heart: cell-based therapies for myocardial repair and regeneration in ischemic heart disease and heart failure. Eur. Heart J. *37*, 1789–1798. https://doi.org/10.1093/eurheartj/ehw113.
40. Bolli, R., Solankhi, M., Tang, X.-L., and Kahlon, A. (2022). Cell therapy in patients with heart failure: a comprehensive review and emerging concepts. Cardiovasc. Res. *118*, 951–976. https://doi.org/10.1093/cvr/cvab135.
41. Carr, C.A., Stuckey, D.J., Tan, J.J., Tan, S.C., Gomes, R.S.M., Camelliti, P., Messina, E., Giacomello, A., Ellison, G.M., and Clarke, K. (2011). Cardiosphere-derived cells improve function in the infarcted rat heart for at least 16 weeks – an MRI study. PLoS One *6*, e25669. https://doi.org/10.1371/journal.pone.0025669.
42. Kasai-Brunswick, T.H., Costa, A.R.d., Barbosa, R.A.Q., Farjun, B., Mesquita, F.C.P., Silva dos Santos, D., Ramos, I.P., Suhett, G., Brasil, G.V., Cunha, S.T.d., et al. (2017). Cardiosphere-derived cells do not improve cardiac function in rats with cardiac failure. Stem Cell Res. Ther. *8*, 36. https://doi.org/10.1186/s13287-017-0481-x.
43. Zhao, Z.-A., Han, X., Lei, W., Li, J., Yang, Z., Wu, J., Yao, M., Lu, X.-A., He, L., Chen, Y., et al. (2018). Lack of cardiac improvement after cardiosphere-derived cell transplantation in aging mouse hearts. Circ. Res. *123*, e21–e31. https://doi.org/10.1161/CIRCRESAHA.118.313005.
44. Lähteenvuo, J., and Rosenzweig, A. (2012). Invited Review: The Role of Angiogenesis in Cardiovascular Aging. Circ. Res. *110*, 1252–1264. https://doi.org/10.1161/CIRCRESAHA.111.246116.
45. Lewis-McDougall, F.C., Ruchaya, P.J., Domenjo-Vila, E., Shin Teoh, T., Prata, L., Cottle, B.J., Clark, J.E., Punjabi, P.P., Awad, W., Torella, D., et al. (2019). Aged-senescent cells contribute to impaired heart regeneration. Aging Cell *18*, e12931. https://doi.org/10.1111/acel.12931.
46. Walaszczyk, A., Dookun, E., Redgrave, R., Tual-Chalot, S., Victorelli, S., Spyridopoulos, I., Owens, A., Arthur, H.M., Passos, J.F., and Richardson, G.D. (2019). Pharmacological clearance of senescent cells improves survival and recovery in aged mice following acute myocardial infarction. Aging Cell *18*, e12945. https://doi.org/10.1111/acel.12945.
47. Yan, C., Xu, Z., and Huang, W. (2021). Cellular Senescence Affects Cardiac Regeneration and Repair in Ischemic Heart Disease. Aging Dis. *12*, 552–569. https://doi.org/10.14336/AD.2020.0811.
48. Solomon, S.D., McMurray, J.J.V., Claggett, B., de Boer, R.A., DeMets, D., Hernandez, A.F., Inzucchi, S.E., Kosiborod, M.N., Lam, C.S.P., Martinez, F., et al. (2022). Dapagliflozin in Heart Failure with Mildly Reduced or Preserved Ejection Fraction. N. Engl. J. Med. *387*, 1089–1098. https://doi.org/10.1056/NEJMoa2206286.
49. Mishra, P.K., Adameova, A., Hill, J.A., Baines, C.P., Kang, P.M., Downey, J.M., Narula, J., Takahashi, M., Abbate, A., Piristine, H.C., et al. (2019). Guidelines for evaluating myocardial cell death. Am. J. Physiol. Heart Circ. Physiol. *317*, H891–H922. https://doi.org/10.1152/ajpheart.00259.2019.
50. Cai, N., Wu, Y., and Huang, Y. (2022). Induction of Accelerated Aging in a Mouse Model. Cells *11*, 1418. https://doi.org/10.3390/cells11091418.
51. Wu, W., Hou, C.-L., Mu, X.-P., Sun, C., Zhu, Y.-C., Wang, M.-J., and Lv, Q.-Z. (2017). H_2S donor NaHS changes the production of endogenous H_2S and NO in D-Galactose-induced accelerated ageing. Oxid. Med. Cell. Longevity *2017*, 5707830. https://doi.org/10.1155/2017/5707830.
52. Chang, Y.-M., Chang, H.-H., Kuo, W.-W., Lin, H.-J., Yeh, Y.-L., Padma Viswanadha, V., Tsai, C.-C., Chen, R.-J., Chang, H.-N., and Huang, C.-Y. (2016). Anti-apoptotic and pro-survival effect of Alpinate Oxyphyllae Fructus (AOF) in a d-Galactose-induced aging heart. Int. J. Mol. Sci. *17*, 466. https://doi.org/10.3390/ijms17040466.
53. Hubesch, G., Hanthazi, A., Acheampong, A., Chomette, L., Lasolle, H., Hupkens, E., Jespers, P., Vegh, G., Wembonyama, C.W.M., Verhoeven, C., et al. (2022). A Preclinical Rat Model of Heart Failure With Preserved Ejection Fraction With Multiple Comorbidities. Front. Cardiovasc. Med. *8*, 809885.
54. Kim, M.Y., Pellot, I., Bresee, C., Nawaz, A., Fournier, M., Cho, J.H., and Cingolani, E. (2023). Diet modification reverses diastolic dysfunction in rats with heart failure and preserved ejection fraction. J. Mol. Cell. Cardiol. *3*, 100031. https://doi.org/10.1016/j.jmccpl.2023.100031.
55. Werner, R.A., Eissler, C., Hayakawa, N., Arias-Loza, P., Wakabayashi, H., Javadi, M.S., Chen, X., Shinaji, T., Lapa, C., Pelzer, T., and Higuchi, T. (2018). Left Ventricular Diastolic Dysfunction in a Rat Model of Diabetic Cardiomyopathy using ECG-gated ^{18}F-FDG PET. Sci. Rep. *8*, 17631. https://doi.org/10.1038/s41598-018-35986-0.
56. Chen, L., Ji, Q., Zhu, H., Ren, Y., Fan, Z., and Tian, N. (2018). miR-30a attenuates cardiac fibrosis in rats with myocardial infarction by inhibiting CTGF. Exp. Ther. Med. *15*, 4318–4324. https://doi.org/10.3892/etm.2018.5952.
57. Liao, P.-H., Hsieh, D.J.-Y., Kuo, C.-H., Day, C.-H., Shen, C.-Y., Lai, C.-H., Chen, R.-J., Padma, V.V., Kuo, W.-W., and Huang, C.-Y. (2015). Moderate exercise training attenuates aging-induced cardiac inflammation, hypertrophy and fibrosis injuries of rat hearts. Oncotarget *6*, 35383–35394.
58. Liu, C., Ni, C., Liu, W., Yang, X., Zhang, R., Zhang, J., Luo, M., Xu, J., and Yu, J. (2021). Effects of long-term nonylphenol exposure on myocardial fibrosis and cardiac function in rats. Environ. Sci. Eur. *33*, 96. https://doi.org/10.1186/s12302-021-00539-2.
59. Schindelin, J., Arganda-Carreras, I., Frise, E., Kaynig, V., Longair, M., Pietzsch, T., Preibisch, S., Rueden, C., Saalfeld, S., Schmid, B., et al. (2012). Fiji: an open-source platform for biological-image analysis. Nat. Methods *9*, 676–682. https://doi.org/10.1038/nmeth.2019.
60. Gómez-Cid, L., Moro-López, M., de la Nava, A., Hernández-Romero, I., Fernández, A., Suárez-Sancho, S., Atienza, F., Grigorian-Shamagian, L., and Fernández-Avilés, F. (2020). Electrophysiological effects of extracellular vesicles secreted by cardiosphere-derived cells: unraveling the antiarrhythmic properties of cell therapies. Processes *8*, 924. https://doi.org/10.3390/pr8080924.
61. Grigorian-Shamagian, L., Fereydooni, S., Liu, W., Echavez, A., and Marbán, E. (2017). Harnessing the heart's resistance to malignant tumors: cardiac-derived extracellular vesicles decrease fibrosarcoma growth and leukemia-related mortality in rodents. Oncotarget *8*, 99624–99636. https://doi.org/10.18632/oncotarget.20454.
62. Konoshenko, M.Y., Lekchnov, E.A., Vlassov, A.V., and Laktionov, P.P. (2018). Isolation of Extracellular Vesicles: General Methodologies and Latest Trends. BioMed Res. Int. *2018*, 8545347. https://doi.org/10.1155/2018/8545347.
63. Ciullo, A., Li, C., Li, L., Ungerleider, K.C., Peck, K., Marbán, E., and Ibrahim, A.G.E. (2022). Biodistribution of unmodified cardiosphere-derived cell extracellular vesicles using single RNA tracing. J. Extracell. Vesicles *11*, e12178. https://doi.org/10.1002/jev2.12178.
64. Lin, Y.-N., Mesquita, T., Sanchez, L., Chen, Y.-H., Liu, W., Li, C., Rogers, R., Wang, Y., Li, X., Wu, D., et al. (2021). Extracellular vesicles from immortalized cardiosphere-derived cells attenuate arrhythmogenic cardiomyopathy in desmoglein-2 mutant mice. Eur. Heart J. *42*, 3558–3571. https://doi.org/10.1093/eurheartj/ehab419.
65. Ibrahim, A.G.-E., Cheng, K., and Marbán, E. (2014). Exosomes as critical agents of cardiac regeneration triggered by cell therapy. Stem Cell Rep. *2*, 606–619. https://doi.org/10.1016/j.stemcr.2014.04.006.
66. Tseliou, E., Fouad, J., Reich, H., Slipczuk, L., de Couto, G., Aminzadeh, M., Middleton, R., Valle, J., Weixin, L., and Marbán, E. (2015). Fibroblasts rendered antifibrotic, antiapoptotic, and angiogenic by priming with cardiosphere-derived extracellular membrane vesicles. J. Am. Coll. Cardiol. *66*, 599–611. https://doi.org/10.1016/j.jacc.2015.05.068.
67. Walravens, A.-S., Smolgovsky, S., Li, L., Kelly, L., Antes, T., Peck, K., Quon, T., Ibrahim, A., Marbán, E., Berman, B., et al. (2021). Mechanistic

and therapeutic distinctions between cardiosphere-derived cell and mesenchymal stem cell extracellular vesicle non-coding RNA. Sci. Rep. *11*, 8666. https://doi.org/10.1038/s41598-021-87939-9.

68. Gómez-Cid, L., López-Donaire, M.L., Velasco, D., Marín, V., González, M. I., Salinas, B., Cussó, L., García, Á., Bravo, S.B., Fernández-Santos, M.E., et al. (2021). Cardiac extracellular matrix hydrogel enriched with polyethylene glycol presents improved gelation time and increased on-target site retention of extracellular vesicles. Int. J. Mol. Sci. *22*, 9226. https://doi.org/10.3390/ijms22179226.
69. Vandesompele, J., De Preter, K., Pattyn, F., Poppe, B., Van Roy, N., De Paepe, A., and Speleman, F. (2002). Accurate normalization of real-time quantitative RT-PCR data by geometric averaging of multiple internal control genes. Genome Biol. *3*, research0034.1. https://doi.org/10.1186/gb-2002-3-7-research0034.
70. White, A.J., Smith, R.R., Matsushita, S., Chakravarty, T., Czer, L.S.C., Burton, K., Schwarz, E.R., Davis, D.R., Wang, Q., Reinsmoen, N.L., et al. (2013). Intrinsic cardiac origin of human cardiosphere-derived cells. Eur. Heart J. *34*, 68–75. https://doi.org/10.1093/eurheartj/ehr172.
71. Perner, S., Brüderlein, S., Hasel, C., Waibel, I., Holdenried, A., Ciloglu, N., Chopurian, H., Nielsen, K.V., Plesch, A., Högel, J., and Möller, P. (2003). Quantifying telomere lengths of human individual chromosome arms by centromere-calibrated fluorescence in situ hybridization and digital imaging. Am. J. Pathol. *163*, 1751–1756. https://doi.org/10.1016/S0002-9440(10)63534-1.
72. Carpentier, G. (2012). Contribution: Angiogenesis Analyzer (ImageJ News).
73. Pascau, J., Gispert, J.D., Soto-Montenegro, M., Rodriguez-Ruano, A., Garcia-Vazquez, V., Udias, A., Vaquero, J.J., and Desco, M. (2007). Small-animal PET registration method with intrinsic validation designed for large datasets. In 2007 IEEE Nuclear Science Symposium Conference Record, pp. 3751–3753. https://doi.org/10.1109/NSSMIC.2007.4436938.

STAR★METHODS

KEY RESOURCES TABLE

REAGENT or RESOURCE	SOURCE	IDENTIFIER
Antibodies		
Anti Ki-67 Antibody	Abcam	Cat# ab15580; RRID: AB_443209
Alexa Fluor Goat anti-rabbit 488 nm	Thermo Fisher	10236882
DAPI	Sigma-Aldrich	D8417
CD105 Antibody, anti-human, PE	Miltenyi Biotec	Cat# 130-112-163; RRID:AB_2654424
CD117 Antibody, anti-human, APC	Miltenyi Biotec	Cat# 130-113-541; RRID:AB_2733335
CD90 Antibody, anti-human, FITC	Miltenyi Biotec	Cat# 130-117-684; RRID:AB_2784296
CD31 Antibody, anti-human, PerCP	Miltenyi Biotec	Cat# 130-110-673; RRID:AB_2657293
CD45 Antibody, anti-human, VioBlue	Miltenyi Biotec	Cat# 130-113-122; RRID:AB_2725950
Biological samples		
Human cardiac biopsies	Hospital Gregorio Marañón	N/A
Chemicals, peptides, and recombinant proteins		
Iscove's Modified Dulbecco's Medium	Hyclone	SH30228
Fetal Bovine Serum	Sigma-Aldrich	F524
Penicillin/Streptomycin	Gibco	15140
2-mercaptoetanol	Gibco	31350
Fibronectin	Sigma-Aldrich	341631
TryPLE Select	Gibco	12563
CryoStor	Sigma-Aldrich	C2894
M-200	Gibco	M200500
Large Vessel Endothelial Supplement	Gibco	A1460801
Low Serum Growth Supplement kit	Gibco	S003K
Geltrex	Thermo Fisher	A1413202
D-gal	Sigma Aldrich	G53688
Critical commercial assays		
QIAzol Lysis Reagent	QIAGEN	79306
iScript™ cDNA Synthesis Kit	Bio-Rad Laboratories	1708890
SYBR® Green chemistry	Bio-Rad Laboratories	172-5124
Abcam's Senescence Detection Kit	abcam	ab65351
Telomere PNA FISH Kit/Cy3	Dako, Agilent	K5326
Human VEGF-A enzyme-linked immunosorbent assay kit	Enzo Life Sciences	156-0001
Human IL-6 enzyme-linked immunosorbent assay kit	Enzo Life Sciences	ADI-900-033
Rat Cytokine Proteome Profiler Array Panel A	R&D Systems	ARY008
Quick Start™ Bradford Protein Assay	Bio-rad	5000201
Deposited data		
Raw and analyzed data	This paper	N/A
Experimental models: Cell lines		
HUVEC	Gibco	C0035C
Experimental models: Organisms/strains		
Rats: Sprague-Dawley	Hospital Gregorio Marañón	N/A
Oligonucleotides		
Primers for genes studied, see Tables S4 and S5	This paper	N/A
Software and algorithms		
ImageJ	Schindelin et al.[59]	https://imagej.net/ij/

(*Continued on next page*)

Continued

REAGENT or RESOURCE	SOURCE	IDENTIFIER
Other		
Ultra-low-attachment Nunclon Plates	Thermo Fisher	174932
Centricon-Plus 70 Centrifugal Filter with 3-kDa cut-off frequency	Merck KGaA	UFC700308
Rapid-Flow Sterile Disposable Filter Units (0.45-μm)	Thermo Fisher	169-0045

EXPERIMENTAL MODEL AND SUBJECT DETAILS

Cardiac biopsies from human subjects

All the studies were conducted according to the guidelines of the Declaration of Helsinki. Human cardiac biopsy collection for EDC, CDC and EV production was approved by the Ethics Committee *Comité de Ética de Investigación con Medicamentos del Hospital General Universitario Gregorio Marañón* (protocol code 331/16 and date of approval 15/12/2016). Informed consent was obtained from all subjects involved in the studies or their legal guardians. Heart tissue was collected from 34 patients who underwent cardiac surgery for other reasons. While adult donors shared the pathology and the disease (mitral valve insufficiency), the disease type varied among pediatric donors (e.g., ventricular or atrial septal defects, Tetralogy of Fallot, mitral insufficiency, Table S2). Patients of both sexes and different ages (including pediatric and adult) were randomly included in the study. Donors' age and sex distribution are detailed in Table S3 and Figure S4.

Generation of EDCs and CDCs

EDCs and CDCs were subsequently obtained following the procedure previously published.[60] In brief, cardiac biopsies from patients undergoing cardiac surgery were processed through mechanical and enzymatic digestion to obtain explants of 1–2 mm size. The explants were cultured and EDCs started leaving the explant and colonizing the plate after approximately 48 h of culture, and they reached full confluency after approximately 16 days. Then, cells were transferred to ultra-low-attachment Nunclon Plates (174932, Thermo Fisher Scientific, Waltham, MA, U.S.A) for 72 h to allow them to form three-dimensional (3D) spheroids (cardiospheres), which are known to potentiate stemness and regenerative potential.[16] The cardiospheres were passaged to produce the CDCs and their identity was confirmed using cell surface markers by flow cytometry (Figure S5).

Animal models

Experiments were approved by the Ethics Committee *Comité de Ética de Experimentación Animal del Hospital Gregorio Marañón* and by the Competent Authority (protocol code 296/19, approved in 2019) conforming to the guidelines from Directive 2010/63/EU of the European Parliament on the protection of animals used for scientific purposes. Rats were housed under standard conditions with free access to food and water. The experimental procedure is illustrated in Figure 5A. Thirty-six 12-week-old Sprague-Dawley rats (30% females) were randomly allocated into four groups: healthy controls (n = 11), D-gal controls (sham group, D-gal, n = 12), D-gal rats treated with more potent CDC-EVs (D-gal + P-EVs, n = 7) and D-gal rats treated with less-potent CDC-EVs (D-gal + NP-EVs, n = 6). To induce cardiac aging, animals in the D-gal groups received during 13 weeks daily intraperitoneal (IP) injections of 600 mg/kg of D-galactose (D-gal, G53688, Sigma Aldrich) resuspended in phosphate buffered saline (PBS) at 300 mg/mL as described.[30] For 13 weeks, animals in the healthy control group received daily IP injections of PBS alone. After 13 weeks, rats in the D-gal group were randomly allocated to receive a single IP administration of the corresponding treatment: 1) PBS alone for the sham group (D-gal); 2) P-EVs resuspended in PBS (D-gal + P-EVs); or 3) NP-EVs resuspended in PBS (D-gal + NP-EVs). The dose of P- and NP-EVs was of 7.5 mg EV equivalent protein/kg animal weight ($\approx 2.25 \cdot 10^{11}$ particles) as based on previous studies.[10,61] During the following 7-weeks, the animals received additional IP injections of D-gal or PBS alone twice a week according to their allocation group to mimic realistic situations of cardiac aging in which after receiving the treatment, factors that affect and increase oxidative stress and cellular damage are still present. In a randomly selected subgroup of rats, cardiac perfusion was evaluated using SPECT at 12 weeks (n = 6) and 19 weeks (n = 18). At the endpoint, blood samples were collected, and the animals were euthanized by cardiac excision under 2% isoflurane anesthesia for further studies. After sacrifice, we determined cardiac hypertrophy and fibrosis, and the gene expression of senescence and fibrosis-related genes (*GLB1*, *TGFB1*, *CDKN2A* and *TP53*).

METHOD DETAILS

Cell culture

Cultured cells were kept incubated at 37°C, 5% CO_2, 21% O_2 and 90% humidity. When cells reached confluency, the cells were detached using TryPLE Select (12563, Gibco) instructions and replated in complete medium or frozen (on CryoStor, C2894, Sigma-Aldrich, at −180°C).

EDCs and CDCs

EDCs and CDCs were obtained and cultured following procedures previously published.[16,60] When cultured and passaged, EDCs and CDCs were seeded over fibronectin coated plates (341631, Sigma-Aldrich, diluted to 12.5 μg/mL in PBS) at a density of 2,000 cells/cm^2 and maintained in Iscove's Modified Dulbecco's Medium (IMDM, SH30228, Hyclone) supplemented 20% with Fetal Bovine Serum (FBS, F524, Sigma-Aldrich), 1% penicillin/streptomycin (PS, 15140, Gibco) and 0.1% 2-mercaptoetanol (31350, Gibco). EDCs and CDC cells reached confluency after approximately 7 days when cultured under these conditions. When doing experiments and obtaining CDC-EVs, the cells were cultured in FBS-free IMDM, keeping the other supplements (PS and 2-mercaptoetanol).

HUVEC

HUVEC (C0035C, Gibco) were passaged and cultured following supplier's instructions. HUVEC were plated over plates at a density of 2,500 cells/cm^2 and maintained in M-200 (Gibco) supplemented with Large Vessel Endothelial Supplement (LVES, A1460801, Gibco) or with the Low Serum Growth Supplement (LSGS) kit (S003K, Gibco). HUVEC reached 80% confluency after approximately 6 days when cultured under these conditions. When doing experiments in HUVEC with the CDC-EVs, the cells were cultured in FBS-free M-200, keeping the addition of the other supplements in the LSGS kit.

Generation and characterization of CDC-EVs

When CDCs from passage 3 (P3) reached approximately 80% confluence, the medium was changed to FBS-free Iscove's Modified Dulbecco's Medium (IMDM), and left unchanged for 15 days to allow CDCs to secrete and concentrate EVs in the medium. Conditioned medium was filtrated using a 0.45-μm filter and ultraconcentrated using Centricon-Plus 70 Centrifugal Filter with 3-kDa cut-off frequency (Merck KGaA, Darmstadt, Germany). The 0.45-μm filter was used to exclude larger particles such as apoptotic bodies[62] from the preparation. EVs were then analyzed by nano-particle tracking analysis (NTA, performed with NanoSight NS300 from Malvern Panalytical Ltd., Malvern, United Kingdom, Figure S5) and their protein content was determined with Bradford assay after EV lysis and protease inactivation. EVs were precipitated after incubation with 4% w/v polyethylene glycol (PEG) overnight at 4°C and centrifugation at 4°C at 1500x g for 30 min. For experiments, the precipitated EVs were resuspended in the corresponding medium at the specified dose. These methods have shown that the isolated EV express typical EV markers such as TSG101,[10,63,64] CD63,[10,63–66] CD81,[63,64,66] HSP90,[63,64] and are negative for calnexin.[63,64] A more detailed expression of the markers found in CDC-EVs can be found in previous works.[67]

Characterization of EDCs and CDCs

During the different stages of product (CDC-EVs) development, involved cells were characterized in terms of their gene expression profile, their biological age and/or their activity as shown in Figure S6. In particular, cellular age in EDCs-P1 (from 18 patients) was measured by the percentage of senescent cells and the expression of some senescence-related genes (*CDKN1A*, *CDKN2A*, and *TP53*). The expression of other genes related to stemness, fibrosis and the secretion of relevant factors for cardiac regeneration and repair was also investigated (*NANOG*, *hTERT*, *GATA4*, *MEF2C*, *TGFB1*, *VEGFA*, *IGF1*, *IGF1R*, *HGF*, *SOD1*, *SOD2*). CDC-P2 identity was confirmed by expression of specific surface markers using flow cytometry (99.0 ± 0.2% CD105+ cells, 8.7 ± 1.6% CD117+ cells, 36.9 ± 3.8% CD90$^+$ cells, 7.2 ± 1.5% CD31$^+$ cells and 1.3 ± 0.2% CD45$^+$ cells, Figure S5A), and CDC-P2 biological age was characterized by the percentage of senescent cells in all donors and by telomere length in 16 donors. Additional CDC-P2 characteristics explored in these 16 donors included proliferation, DNA synthesis, migration and VEGF-A secretion.

Senescence

Cells were plated in complete medium (3 wells per condition/donor) at 13,000 cells/cm^2 in fibronectin pre-coated 12-well plates. After 24 hour-incubation, wells were washed and replaced with FBS-free medium (containing the resuspended CDC-EVs if applicable). After another 72 hour-incubation, the cells were fixed using Abcam's Senescence Detection Kit (ab65351, abcam, Cambridge, UK), which is used to detect SA-β-Gal activity in cultured cells. The samples were prepared, fixed and stained following the assay protocol (with overnight incubation). After staining, samples were washed and kept in 70% glycerol (G5516, Sigma-Aldrich) in PBS at 4°C. As SA-β-Gal positive cells develop a blue color, a total of around 10 images at 20x (around 650 cells) per well were taken with a Leica DMI3000B optical microscope and Leica DFC310 FX camera (Wetzlar, Germany), and manually classified as senescent (blue) or non-senescent using ImageJ Software[59] and as previously described.[68]

Gene expression analysis. EDCs-P0 from 18 donors were characterized in terms of the relative gene expression of specific genes involved in stemness, fibrosis, the secretion of relevant factors and senescence. The genes under study were: *NANOG*, *hTERT* and *GATA4, MEF2C, TGFB1, VEGF, IGF1, IGF1R, HGF, SOD1, SOD2, CDKN1A, CDKN2A,* and *TP53*. RNA from 300,000 pelleted EDCs-P0 was isolated using QIAzol Lysis Reagent instructions (QIAGEN, Venlo, The Netherlands) and relative gene expression quantification was performed with a two-step Real-Time Polymerase Chain Reaction (RT-PCR, in a MyCycler Thermal Cycler System, Bio-Rad Laboratories, Hercules, CA, U.S.A). One microgram of total RNA was reverse-transcribed into complementary DNA (cDNA) using the iScript cDNA Synthesis Kit (1708890, Bio-Rad Laboratories) and random hexamer primers in 20-μL reactions, following the manufacturer's instructions. cDNA obtained was diluted 1:20 and gene expression quantification was performed in a CFX RT-PCR Detection System (Bio-Rad Laboratories) using a 96-well plate and each sample was analyzed in triplicate. PCR amplifications were done with 2 μL of diluted cDNA using SYBR Green chemistry (172-5124 Bio-Rad Laboratories) and specific primer pairs in a final volume of 20 μL. RT-qPCR efficiency for each assay was controlled using relative standard

curves generated from a pool of cDNA. Ct data was collected and analyzed applying the $2^{-\Delta\Delta Ct}$ method for relative quantification using the sample with the highest expression as calibrator. Gene expression normalization factor was calculated for each sample based on the geometric mean of *GADPH* and *18S* reference genes in geNorm.[69] Specific primer pairs are detailed in Table S4.

Flow cytometry. For flow cytometry, 150,000 CDCs-P1 from 16 donors were plated in a 100 mm dish and cultured until full confluency (around one week) in complete medium. Cells were detached using TryPLE Select (12563, Gibco) instructions, counted (around 500,000) and resuspended in 500 μL of PBS. Corresponding antibodies (CD105 PE, CD117 APC, CD90 FITC, CD31 PerCP and CD45 Vioblue from Miltenyi Biotec) were added to the cell suspension and incubated during 15 min at Room Temperature (RT) in the absence of light. Immunofluorescence was quantified with a MACSQuant (Miltenyi-Biotech, Bergisch Gladbach) cytometer and data analyzed using Macs Quantify software. The average percentage of CDC-P2 from the different donors expressing each of the explored surface markers is summarized in Figure S5A: 99.0 ± 0.2% CD105+ cells, 8.7 ± 1.6% CD117+ cells, 36.9 ± 3.8% $CD90^+$ cells, 7.2 ± 1.5% $CD31^+$ cells and 1.3 ± 0.2% $CD45^+$ cells, in concordance to the population of CDCs described by other groups.[16,17,70]

DNA synthesis

CDC cultures for immunocytochemistry analysis were washed in PBS and fixed in 4% formaldehyde for at least 24 h. For analyzing DNA synthesis, fixed cells were washed three times in PBS and permeabilized with 0.1% Triton-X (X100, Sigma-Aldrich) in PBS for 30 min at RT. They were later kept 1 h at RT with Dako protein block (X0909, Dako), and overnight incubated in the Ki-67 primary antibody (ab15580, abcam) at a dilution of 1:400 in Dako protein block and 4°C in a humid chamber. After three 10 min washes, the samples were left in Alexa Fluor Goat anti-rabbit 488 nm antibody (10236882, Thermo Fisher Scientific, Waltham, MA, U.S.A) at 1:400 in Dako protein block 1 h at RT, washed twice, incubated in DAPI (D8417, Sigma-Aldrich) at 1:5000 in PBS 10 min at RT, washed twice and kept in PBS at 4°C until imaging. Around 10 images at 10x per well (800–1200 cells) were acquired with the Leica DMI3000B optical microscope and Leica DFC310 FX camera (Wetzlar, Germany), and analyzed using ImageJ Software.

Proliferation. CDCs-P1 from 16 donors were plated at 4,200 cells/cm^2 in 6-well plates (3 wells per condition/donor) in complete medium. After 24 h (time 0), each well was washed with PBS, changed to FBS-free medium, an imaged at eight random locations previously marked at 5x with the Leica DMI3000B optical microscope and Leica DFC310 FX camera (Wetzlar, Germany). After another 72 h, wells were imaged at the exact same locations with the same parameters. Cells in each image were manually counted using ImageJ, and Population Doubling Time (PDT) at each location was calculated according to Equation 1. Average PDT was obtained from the PDT at each of the 24 locations.

$$PDT = (t_2 - t_1) * \frac{\log(2)}{\log(q2) - \log(q1)} \quad \text{(Equation 1)}$$

Population Doubling Time. $t_2 - t_1$ is equal to the elapsed time, in this case 3 days. $q2$ is the final number of cells, in this case, after the 72 hours. $q1$ is the initial number of cells.

Migration. CDCs-P1 were plated at 57,000 cells/cm^2 in 12-well plates (3 wells per donor) in complete medium. After 24 h, wells were washed, changed to FBS-free medium and incubated for 48 h. Wounds were generated using a 1000 μL pipette tip, washed, and imaged at 5x in five different marked locations per well with the Leica DMI3000B optical microscope and Leica DFC310 FX camera (Wetzlar, Germany). After 24 h, wounds were imaged at the same locations. Images were processed in ImageJ to determine the percentage of wound closure. First, the wound area at the time of wound generation (time 0) was determined. Then, cells in that same area were segmented in the image taken at the same location after 24 h. The percentage of wound closure was calculated at each location as the area of the segmented cells divided by the total area of the wound. The average percentage of wound closure for CDCs of each donor was obtained by averaging the value in the 15 locations.

Telomere length. CDC-P2 nucleus telomere length was analyzed with the Telomere PNA FISH Kit/Cy3 (K5326, Dako, Agilent, Santa Clara, CA, U.S.A). 150,000 CDCs-P1 from 16 donors were plated in a 100 mm dish and cultured until full confluency (around one week) in complete medium. Cells were detached using TryPLE Select (12563, Gibco) instructions, counted (250,000–500,000), pelleted and resuspended in 9 mL of KCl 75 mM in H_2Od. After 30 min incubation at 37°C, nuclei were fixed and washed in Carnoy's solution (methanol and acetic acid 3:1) and stored at 4°C until hybridation. Fixed nuclei were pre-treated, denatured and hybridized, washed and counterstained following the kit instructions and stored at −20°C until imaging. A minimum of 50 nuclei from each donor were imaged at 63.5x keeping the same image parameters with a confocal scanning inverted AOBS/SP2-microscope (Leica Microsystems, Wetzlar, Germany) and analyzed using ImageJ software. After background subtraction, nuclei were segmented in the corresponding DAPI image. The mean intensity value of each segmented nucleus was calculated in the Cy3 image, as the length of the telomeres is directly correlated to the fluorescence intensity of the spots.[71]

VEGF-A secretion. CDCs-P1 from 16 different donors were plated in triplicate at 28,500 cells/cm^2 in 12-well plates in complete medium. After 24 h, each well was washed with PBS and incubated with 600 μL of FBS-free media for 72 h. After this time, the conditioned media was collected and the VEGF secretion analyzed following the VEGF enzyme-linked immunosorbent assay (ELISA) kit instructions from Enzo Life (156-0001, Enzo Life Sciences, Farmingdale, NY, U.S.A).

Design of the ageing-reversal potency matrix assay

The obtained CDC-EV were characterized in terms of their bio-activity using an ageing-reversal potency matrix assay. In particular, the rejuvenating and pro-angiogenic potency was tested *in vitro* on EDCs previously obtained and endothelial cells (ECs, HUVEC,

C0035C, Gibco). EDCs were used as the target Cardiac Stromal Cell (CSC) population as they contain a variety of cell types important in heart physiology and pathology.[16,17] Two types of CSCs were used as target: moderately senescent (25.6 ± 1.4% of senescent cells in culture) from target donor 1 (54 years old, male) and highly senescent (47.5 ± 1.3%) from target donor 2 (56 years old, female). The rejuvenating potency of CDC-EVs was determined by their ability to reduce CSC senescence, to induce CSC IL-6 secretion and to reduce the gene expression of *CDKN1A* (p21), *CDKN2A* (p16), *TP53* (p53) and *TGFB1* (TGF-β), senescence and fibrosis-related genes in CSCs. Senescence reduction induced by the different CDC-EVs in the CSCs of each target donor was calculated by subtracting the average percentage of senescent cells in the CSC after adding the different CDC-EVs in SFM minus the average percentage of senescent cells in the donor under control conditions (SFM alone). Therefore, the more negative the value obtained, the more the CDC-EVs reduced senescence. The same formula was used for estimating the increment in IL-6 secretion induced by the CDC-EVS. The more positive the value obtained, the more the CDC-EVs induced IL-6 secretion. The CDC-EV pro-angiogenic potency was determined by their ability to induce tube formation on HUVEC, dividing the average total branching length of the ECs with the different CDC-EVs by the total branching length of the ECs under control conditions (SFM alone). A value higher than one means the CDC-EVs were able to increase EC tube formation, while a value smaller than one means the CDC-EVs impaired EC tube formation compared to control conditions.

The results of all the tests in the matrix-assay for each CDC-EVs were scored individually and added to estimate the global potency score as shown in Table S1. Each test related to function modification (ability to reduce senescence, to induce increases in IL-6 secretion and to induce EC tube formation) was assigned a maximum score of 2 (more weight in the final score), whereas each test related to the ability to modify gene expression of senescence or fibrosis markers received half of the weight in the final score (a maximum possible score of 1). In each test, the CDC-EVs were divided in three groups: the ones showing superior performance (6/18, first tercile) that received the maximum possible score for that particular test, the ones showing average performance (second tercile) receiving half of the maximum score for that particular test, and the ones showing the worst performance (third tercile) receiving no score for the corresponding test. The CDC-EVs with the highest total score were selected as more-potent (P-EV) and the CDC-EVs with the total lowest score were selected as less-potent (NP-EV). The maximum possible score was 18 if CDC-EVs showed superior performance in all the tests in the matrix-assay.

Anti-senescent effect

CSCs were plated in complete medium at 13,000 cells/cm^2 in fibronectin pre-coated 12-well plates. After 24 hour-incubation, wells were washed and replaced with FBS-free medium (blank or containing the resuspended CDC-EVs). After another 72 hour-incubation, the cells were fixed using Abcam's Senescence Detection Kit following the assay protocol. All samples were run in triplicate. Senescence reduction of the different CDC-EVs was calculated as senescence of EDCs-P3 from donor 1 (25.6 ± 1.4%) or donor 2 (47.5 ± 1.3%) treated with the corresponding CDC-EVs minus the senescence of the EDCs-P3 of the same donor under control conditions (SFM alone, 25.6% in donor 1 and 47.5% in donor 2). The more negative the value obtained, the more the CDC-EVs reduced senescence.

Gene expression reduction

The gene expression of senescence and fibrosis-related genes (*CDKN1A* (p21), *TGFB1* (TGF-β), *CDKN2A* (p16) and *TP53* (p53)) in target CSCs under control conditions or treated with the CDC-EVs from the eighteen different donors were analyzed. CSCs were plated in complete medium at 13,000 cells/cm^2 in fibronectin pre-coated 12-well plates. After 24 hour-incubation, wells were washed and replaced with FBS-free medium (blank or containing the resuspended CDC-EVs). After another 72 hour-incubation, RNA was isolated, reverse-transcribed into cDNA, PCR amplified and the gene expression quantified as previously described. Specific primer pairs are detailed in Table S4. All samples were run in triplicate. The relative expression of each gene in the CSCs under the effect of the different CDC-EVs was normalized by the expression of the same gene in the untreated CSCs.

IL-6 secretion

CSCs were plated in complete medium at 13,000 cells/cm^2 in fibronectin pre-coated 12-well plates. After 24 hour-incubation, wells were washed and replaced with 600 μL of FBS-free medium (blank or containing the resuspended CDC-EVs). After another 72 hour-incubation, the conditioned media was collected, diluted 1:25, and IL-6 levels determined following the kit instructions from Enzo Life (ADI-900-033, Enzo Life Sciences, Farmingdale, NY, U.S.A). All samples were run in triplicate. Increment in IL-6 secretion caused by CDC-EVs was calculated as IL-6 secretion of EDCs-P3 from donor 1 or donor 2 under the effect of the different CDC-EVs minus the IL-6 secreted by the untreated EDCs (140 ± 6.6 pg/mL in donor 1 and 291 ± 26 pg/mL in donor 2).

Pro-angiogenic effect

The pro-angiogenic effect of the different CDC-EVs was tested as their ability to induce tube formation. 12-well plates were coated with 150 μL of Geltrex (A1413202, Thermo Fisher Scientific, Waltham, MA, U.S.A) and incubated at 37°C for 30 min. Later, 87,500 HUVEC-P5 were resuspended in 500 μL of FBS-free M-200 (negative control), in M-200 with FBS (positive control) or in FBS-free M-200 with the CDC-EVs at 300 μg (≈9·10^9 particles)/1·10^6 cells and plated over the pre-coated plates in three wells for each condition. After 15 h of incubation, tube formation was imaged at 5x in 5–6 different locations in each well with the Leica DMI3000B optical microscope and Leica DFC310 FX camera (Wetzlar, Germany). 16–20 images per condition were analyzed and quantified automatically using the Angiogenesis Analyzer tool in ImageJ[72] and used to obtain the average total branching length. The relative tube formation of HUVEC treated with the different CDC-EVs was obtained by normalizing the total branching length by the total branching

length of HUVEC with FBS-free-medium (and without any CDC-EVs). A value higher than one means the CDC-EVs were able to increase EC tube formation, while a value smaller than one means the CDC-EVs impaired EC tube formation compared to control conditions.

In vivo evaluation

Gene expression analysis

The gene expression of senescence and fibrosis-related genes (*GLB1* (β-galactosidase) and *TGFB1* (TGF-β)) in the cardiac tissue of the rats in the different groups was analyzed as previously described, but using *ACTB* as reference gene for gene expression normalization. Specific primer pairs are detailed in Table S5. The number of animals in each group that underwent the cardiac gene expression analysis were: Healthy: $n = 6$, D-gal: $n = 11$, D-gal + P-EVs: $n = 7$, D-gal + NP-EVs: $n = 6$.

Cardiac hypertrophy

Cardiac hypertrophy was determined at the endpoint by calculating the ratio between the heart weight (mg) and the body weight (g). For determining heart weight, hearts were carefully cleaned and washed from major vessels, blood, and clots in PBS. The hearts were weighted after removing excess fluid. The number of animals in each group that were included in the cardiac hypertrophy measurement were: Healthy: $n = 8$, D-gal: $n = 12$, D-gal + P-EVs: $n = 7$, D-gal + NP-EVs: $n = 6$.

Cardiac fibrosis

Excised hearts were fixed in 4% formaldehyde at least for one month and a tissue portion in the medium region of the ventricles dehydrated and embedded in paraffin blocks. This was done with a Myr STP120 (Tarragona, Spain) tissue processor with the following program: (i) 3 times, 1 h each, in 96% ethanol (ii) 3 times, 1 h each, in 100% ethanol (iii) 3 times, 1 h each, in isoparaffin, and (iv) twice, 2 h each, in paraffin, followed by inclusion with a Myr EC350-1 modular tissue embedding center. The blocks were cut into 3 μm slices with a microtome (Microm HM325, Thermo Scientific), mounted, and fixed to the glass slide with heat (90°C for 1 h followed by 60°C for 2 h). The slices were later deparaffined (embedding in isoparaffin during 60 s while shaking) and hydrated (embedding in 100% ethanol during 60 s while shaking, the same procedure in 96% ethanol, and in distilled water). The slices were finally stained with Masson's Trichrome staining using the reagents and the procedure from Bio-Optica. The slides were mounted and imaged with a Leica DM 1000 LED microscope (8 random images per heart, in interstitial sites, at 20x) and manually segmented for estimating the percentage of fibrotic area (in blue) using ImageJ. The number of animals in each group that were included in the cardiac fibrosis measurement were: Healthy: $n = 4$, D-gal: $n = 12$, D-gal + P-EVs: $n = 7$, D-gal + NP-EVs: $n = 6$.

Cardiac perfusion

ECG-gated SPECT images were performed with a small-animal scanner (μSPECT, MILabs, the Netherlands) 60 min after the intravenous administration of 65.7 ± 11.9 ^{99m}Tc-sestamibi. The SPECT acquisition parameters were an isotropic voxel size of 0.4 mm and 1 h of acquisition time, images were reconstructed using two-dimensional ordered subset expectation maximization (OSEM-2D) with 16 subsets and 1 iteration. For manual analysis, Multimodality Workstation software (MMWKS)[73] was used to define LV myocardium by a single expert to get the mean, maximum and minimum of ^{99m}Tc-sestamibi uptake values. The number of animals in each group that underwent the cardiac perfusion study before receiving the treatment were: D-gal + P-EVs: $n = 4$, D-gal + NP-EVs: $n = 2$. The number of animals in each group that underwent the cardiac perfusion study at the endpoint were: Healthy: $n = 4$, D-gal: $n = 4$, D-gal + P-EVs: $n = 6$, D-gal + NP-EVs: $n = 4$. To prepare the images for Figures 5F and S3A, intensity of representative raw SPECT images was normalized by the injected dose, by the animal weight and by the acquisition time using ImageJ to allow for comparison. From the normalized 3D image, a slide in the middle of the LV was chosen and displayed using the physics look up table with the same window and level in the images of the different animals.

Cytokine concentration in peripheral blood

Blood collected at the endpoint on serum tubes was left at RT for 30 min and then centrifuged at 2000× g at 4°C for 15 min. Serum was stored at −80°C until used. The samples were assessed using the Rat Cytokine Array Panel A from R&D Systems (ARY008, Minneapolis, USA) following manufacturer's instructions. The number of animals in each group that underwent the cytokine concentration test were: Healthy: $n = 4$, D-gal: $n = 4$, D-gal + P-EVs: $n = 4$, D-gal + NP-EVs: $n = 4$.

QUANTIFICATION AND STATISTICAL ANALYSIS

Results are presented as mean ± standard error of the mean (SEM) in the text and in figures. Significance of differences was assessed by Student's t test or with 1-way ANOVA in case of multiple groups if the distribution of the variable was normal; otherwise, the Mann-Whitney or Kruskal-Wallis tests were used. Categorical variables (percentage of senescent cells and of Ki-67+ cells) were compared using the *Z* Score for two population proportions. Pearson tests were performed to study the correlation among the different parameters. All probability values reported are two-sided, with $p < 0.05$ considered significant. For *in vitro* studies the lowest number of replicates per experiment was three.

ADDITIONAL RESOURCES

Human samples collection was approved by the Ethics Committee *Comité de Ética de Investigación con Medicamentos del Hospital General Universitario Gregorio Marañón* (protocol code 331/16 and date of approval 15/12/2016).